CANCER

Discovery of DRP-104, a tumor-targeted metabolic inhibitor prodrug

Rana Rais[1,2,3]*, Kathryn M. Lemberg[1,4], Lukáš Tenora[1,5], Matthew L. Arwood[6], Arindom Pal[1,2], Jesse Alt[1], Ying Wu[1], Jenny Lam[1], Joanna Marie H. Aguilar[1], Liang Zhao[4,6], Diane E. Peters[1,3], Carolyn Tallon[1,2], Rajeev Pandey[4], Ajit G. Thomas[1], Ranjeet P. Dash[1,2], Tanguy Seiwert[4], Pavel Majer[5], Robert D. Leone[4,6], Jonathan D. Powell[3,4,6], Barbara S. Slusher[1,2,3,4,6,7,8,9]*

6-Diazo-5-oxo-L-norleucine (DON) is a glutamine antagonist that suppresses cancer cell metabolism but concurrently enhances the metabolic fitness of tumor CD8$^+$ T cells. DON showed promising efficacy in clinical trials; however, its development was halted by dose-limiting gastrointestinal (GI) toxicities. Given its clinical potential, we designed DON peptide prodrugs and found DRP-104 [isopropyl(*S*)-2-((*S*)-2-acetamido-3-(1*H*-indol-3-yl)-propanamido)-6-diazo-5-oxo-hexanoate] that was preferentially bioactivated to DON in tumor while bioinactivated to an inert metabolite in GI tissues. In drug distribution studies, DRP-104 delivered a prodigious 11-fold greater exposure of DON to tumor versus GI tissues. DRP-104 affected multiple metabolic pathways in tumor, including decreased glutamine flux into the TCA cycle. In efficacy studies, both DRP-104 and DON caused complete tumor regression; however, DRP-104 had a markedly improved tolerability profile. DRP-104's effect was CD8$^+$ T cell dependent and resulted in robust immunologic memory. DRP-104 represents a first-in-class prodrug with differential metabolism in target versus toxicity tissue. DRP-104 is now in clinical trials under the FDA Fast Track designation.

INTRODUCTION

Many of the most effective antineoplastic agents are antimetabolites, which block the altered metabolism of tumor cells (*1*, *2*). The rapid growth of tumor cells creates enormous metabolic demand for energy and substrates for protein and nucleic acid synthesis. Among the altered pathways, glutamine metabolism plays a prominent role in providing carbon and nitrogen building blocks, turning tumors into "glutamine sinks" that exhibit a high rate of glutamine consumption in comparison to normal tissues (*3*, *4*). Glutamine metabolism is reprogrammed by cancer mutations, including those in the MYC, TP53, Ras-related oncogenes, LKB1-AMP (adenosine monophosphate) kinase (AMPK), and phosphatidylinositol 3-kinase (PI3K) pathways (*5*, *6*). Glutamine functions as an energy source via the tricarboxylic acid (TCA) cycle and supplies carbon and nitrogen as precursors for amino acid, lipid, and nucleotide synthesis and for the maintenance of redox balance (*7*). Thus, globally blocking glutamine utilization in cancer cells has substantial therapeutic potential (*8*, *9*).

6-Diazo-5-oxo-L-norleucine (DON) shares high structural similarity to glutamine and selectively blocks multiple glutamine-using reactions. Mechanistically, DON contains an α-diazoketone, which is activated by proton transfer within the active site of a glutamine-using enzyme (e.g., in the proximity of the active-site serine residue in glutaminase) (*10*), forming a carbocation that reacts instantly with the enzyme such that no reactive species is released. Therefore, DON does not simply serve as a standard irreversible inhibitor, but rather a selective, mechanism-based inactivator of glutamine-using enzymes, including carbamoyl phosphate synthase, cytidine triphosphate synthase, phosphoribosyl formylglycinamidine synthetase (PFAS), guanosine monophosphate synthetase, phosphoribosyl pyrophosphate aminotransferase, nicotinamide adenine dinucleotide synthase, asparagine synthase, and glutaminase, which collectively serve vital roles in the TCA cycle, purine, lipid, hexosamine, and amino acid synthetic pathways (*11*–*17*). Not only does DON effectively block tumor glutamine utilization but we also recently found that DON has divergent metabolic effects on tumor cells versus effector T cells, resulting in simultaneous starvation of the tumor cells and enhancement of the cytotoxic effects of T cells in the tumor microenvironment (*18*). The distinctive combination of depleting tumors of nutrients while enhancing T cell function makes glutamine antagonism an exceptionally promising therapeutic strategy.

DON has shown remarkable antitumor efficacy in preclinical and clinical studies (*19*–*31*). For example, in one of the first clinical studies using DON, 31 of 47 patients (66%) who received 2 weeks or more of DON therapy demonstrated stable disease or regression (*19*). When dosed in children with hematological malignancies on standard 6-mercaptopurine therapy, DON supplementation led to substantially better bone marrow remissions (*32*). Unfortunately, broad metabolic inhibitors like DON exhibit toxicity in healthy tissues that also have a high metabolic demand for glutamine. For example, the gastrointestinal (GI) system is highly dependent on glutamine for regulating cell proliferation and repair and maintaining gut barrier functions (*33*). Consequently, clinical development of DON was abandoned due to its dose-limiting toxicities to normal tissues, many of which were GI-related (e.g., mucositis, diarrhea, and gastric bleeding) (*19*, *21*, *22*). Selective inhibitors of certain glutamine pathways, such as allosteric glutaminase inhibitors, have been tested but fail to show robust clinical efficacy (*34*), perhaps because of the adaptation of tumors through alternate metabolic pathways.

[1]Johns Hopkins Drug Discovery, Johns Hopkins School of Medicine, Baltimore, MD 21205, USA. [2]Department of Neurology, Johns Hopkins School of Medicine, Baltimore, MD 21205, USA. [3]Department of Pharmacology and Molecular Sciences, Johns Hopkins School of Medicine, Baltimore, MD 21205, USA. [4]Department of Oncology, Johns Hopkins School of Medicine, Baltimore, MD 21205, USA. [5]Institute of Organic Chemistry and Biochemistry, Academy of Sciences of the Czech Republic v.v.i., Prague 16000, Czech Republic. [6]The Bloomberg-Kimmel Institute for Cancer Immunotherapy, Johns Hopkins School of Medicine, Baltimore, MD 21287, USA. [7]Department of Psychiatry and Behavioral Sciences, Johns Hopkins School of Medicine, Baltimore, MD 21205, USA. [8]Department of Neuroscience, Johns Hopkins School of Medicine, Baltimore, MD 21205, USA. [9]Department of Medicine, Johns Hopkins School of Medicine, Baltimore, MD 21205, USA.
*Corresponding author. Email: bslusher@jhmi.edu (B.S.S.); rrais2@jhmi.edu (R.R.)

We hypothesized that a broader metabolic inhibitor that could be targeted preferentially to the tumor environment may offer a strategic approach for improving the therapeutic index of this class of drugs.

Prodrug strategies have been widely used to modify distribution and improve the delivery of active agents to target tissues (*35*). We sought to develop a DON prodrug that could selectively deliver DON to tumor tissues while sparing normal glutamine-dependent tissues like the GI tract. We previously reported the synthesis and preclinical evaluation of a DON prodrug with enhanced central nervous system–to–plasma distribution in both swine and primates (*36*, *37*), showing the feasibility of this targeting strategy. On the basis of a similar principle, we used a discrete chemical approach to design tumor-targeted prodrugs of DON using promoieties that could be cleaved by enzymes enriched in the tumor (*38*).

Cumulative evidence suggests that tumors express enriched protease activity; many proteases have been identified as cancer biomarkers (*38*–*40*). We hypothesized that modification of DON to a "peptide prodrug" would enable its preferential bioactivation by the tumor-enriched proteases, thus sparing the normal tissue. Systematic synthesis and characterization of a series of DON prodrugs led to the discovery of DRP-104 [isopropyl(*S*)-2-((*S*)-2-acetamido-3-(1*H*-indol-3-yl)-propanamido)-6-diazo-5-oxo-hexanoate], a prodrug carrying two promoieties—an isopropyl ester and an acetylated tryptophan on DON's carboxylate and amine, respectively. We report here that DRP-104 administration to CES1$^{-/-}$ mice (a model recapitulating human prodrug metabolism) resulted in prodigious 6- and 11-fold greater exposures of DON to the tumor versus plasma and GI tissue, respectively, resulting in complete tumor regression without GI side effects. We further showed that DRP-104 enhanced the efficacy of anti-PD-1 immunotherapy and that its effect was CD8^{+} T cell dependent. Last, and most remarkably, we showed that mice previously cured with DRP-104 monotherapy completely rejected tumor rechallenge, indicating that glutamine antagonism therapy triggers immunologic memory. On the basis of these promising preclinical data, DRP-104 is currently in clinical trials (NCT04471415) for treatment of advanced-stage solid tumors as a single agent and in combination with immunotherapy.

RESULTS

Synthesis of DON prodrugs and the discovery of DRP-104

The structures of glutamine, DON, DRP-104, and its de-esterified M1 metabolite are illustrated in Fig. 1. The synthetic schemes, reaction conditions, structure of DRP-104 (P3) and related prodrugs (P1–2 and P4–8), as well as their characterization are shown in figs. S1 and S2 (A to C). The synthetic schemes and reaction conditions for the M1 metabolite are shown in fig. S3. DON shows high structural similarity to glutamine. The difference is that the amine in glutamine is replaced with a diazo group in DON that enables irreversible binding and mechanism-based inactivation of glutamine-using enzymes. In support of this, we show that DON dose-dependently inhibits the glutaminase enzyme (GLS-1) with an IC_{50} (median inhibitory concentration) of 10 ± 0.3 μM (table S1), similar to that reported in literature (*41*). DRP-104 is a peptide prodrug of DON with an acetylated tryptophan moiety on the amine and an isopropyl ester on the DON carboxylic acid. As an intact prodrug, DRP-104 is inactive as an inhibitor of glutamine-using enzymes, including GLS-1 (table S1), as enzymatic bioactivation to DON is required for activity. Similarly, DRP-104's de-esterified M1 metabolite is also inactive (table S1). Of the multiple DON prodrugs (P1 to P8) synthesized and evaluated, DRP-104 (P3) showed the most promising initial metabolic stability, DON release, and tumor partitioning results (fig. S2) and was selected for further characterization.

DRP-104 is bioactivated in the tumor while bioinactivated in GI tissue, resulting in preferential DON delivery to tumors

DRP-104 stability was evaluated in wild-type (WT) and C57BL/6/CES1$^{-/-}$ mouse and human plasma (Fig. 2A). While DRP-104 was completely unstable in WT C57BL/6 mouse plasma (0% remaining at 60 min), it exhibited good stability in both C57BL/6/CES1$^{-/-}$ mouse and human plasma (>90% remaining at 60 min). Notably, this interspecies difference in metabolism is not uncommon in prodrug discovery. It is well established that carboxylesterase enzyme 1 (CES1) is highly abundant in rodent plasma but not present in higher species plasma, specifically human plasma (*42*). To mimic this phenomenon, C57BL/6/CES1$^{-/-}$ mice were generated by inactivating the CES1 gene such that there was undetectable CES activity in plasma but normal activity in tissues (*43*), making these mice a better preclinical model to mimic human metabolism. Stability was also evaluated in intestinal tissue homogenate (mouse) and intestinal S9 fractions (human). In both intestinal matrices, DRP-104 was unstable (0% remaining at 60 min; Fig. 2B), predominantly showing hydrolysis to a charged and inactive intermediate metabolite M1 (Fig. 1 and fig. S4) with <10% DON release (Fig. 2C).

Next, to validate that DRP-104 was bioactivated in tumor cells and that its antiproliferative effects were arising from DON release, equimolar DRP-104, DON, M1, and P1 were assessed in a P493B lymphoma cell viability assay. Dose-dependent decrease in cell proliferation was observed with DON and DRP-104 with EC_{50} (median effective concentration) values of 4.0 ± 0.6 and 10 ± 1.9 μM, respectively (fig. S5). In contrast, MI and P1, which do not release DON (figs. S2C and S4), showed no effect on cell viability (fig. S5).

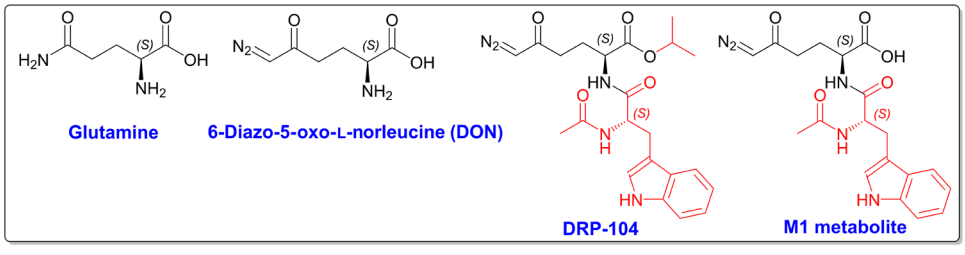

Fig. 1. Chemical structures of glutamine, DON, DRP-104, and M1 metabolite. Synthesis and characterization are reported in figs. S1 and S3.

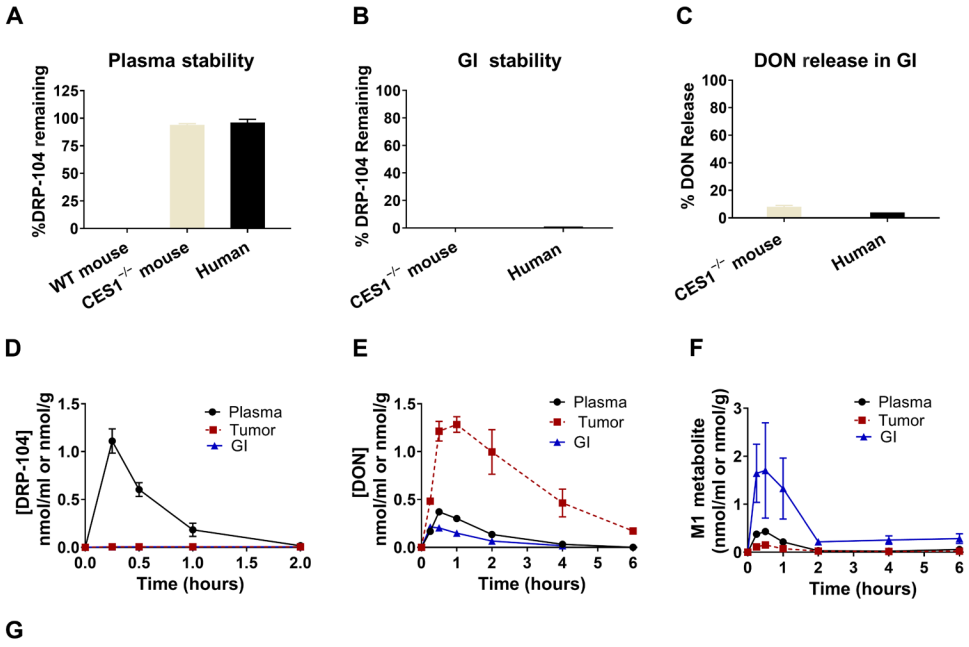

G

Pharmacokinetic parameters					
Compound	Matrix	C_{max} (nmol/ml or nmol/g)	T_{max} (hours)	$AUC_{0\text{-}t}$ (nmol hour/ml or nmol hour/g)	Tumor penetration index ($AUC_{0\text{-}t\ (tumor/tissue)}$)
DRP-104	Plasma	1.11 ± 0.13	0.25	0.65 ± 0.08	n.c.
	Tumor	BLQ	n.c.	n.c.	n.c.
	GI	BLQ	n.c.	n.c.	n.c.
DON	Plasma	0.37 ± 0.03	0.5	0.67 ± 0.09	6.20
	Tumor	1.28 ± 0.08	1	4.13 ± 0.59	—
	GI	0.21 ± 0.12	0.25	0.36 ± 0.13	11.5
M1 metabolite	Plasma	0.42 ± 0.03	0.5	0.56 ± 0.09	0.39
	Tumor	0.15 ± 0.01	0.5	0.22 ± 0.02	—
	GI	1.7 ± 0.12	0.5	3.2 ± 0.85	0.07

Fig. 2. DRP-104 shows activation to DON in tumor and inactivation to M1 metabolite in GI tissues. (**A**) DRP-104 stability in WT mice, C57BL/6/CES1$^{-/-}$ mice, and human plasma and (**B**) GI tissues (jejunum for mice and S9 for human) showing that stability of DRP-104 in C57BL/6/CES1$^{-/-}$ mice mimics human metabolism. (**C**) Although DRP-104 is unstable in GI tissues, minimal DON is liberated. DRP-104 (1 mg/kg DON equivalent, subcutaneously) was administered to C57BL/6/CES1$^{-/-}$ mice bearing EL4 flank tumors; tissues were harvested and analyzed for (**D**) DRP-104, (**E**) DON, and (**F**) M1 metabolite. Following DRP-104 administration, DON exposures were 6- and 11-fold higher in the tumor when compared to plasma and GI tissues, respectively. DRP-104 was detected in plasma but not in tumor or GI tissue. (**G**) PK parameters of DRP-104, DON released from DRP-104, and the M1 metabolite in plasma, tumor, and GI tissues, with data expressed as means or means ± SEM ($n = 3$ per time point). BLQ, below limit of quantification; n.c., not calculated.

Given its desirable in vitro profile (i.e., stable in plasma, minimal DON release in GI tissue, excellent tumor cell partitioning, and cytotoxic effect on tumor cells), DRP-104 pharmacokinetics were evaluated in vivo using C57BL/6/CES1$^{-/-}$ mice bearing EL4 flank tumors. DRP-104 was administered subcutaneously at a dose of 2.6 mg/kg (1 mg/kg DON equivalent), and subsequently, plasma, tumor, and intestinal tissues were collected and analyzed for DRP-104, DON, and its de-esterified M1 metabolite (Fig. 2, D to F) using our validated liquid chromatography–mass spectrometry (LC-MS) methods (*36*, *37*, *44*). Intact DRP-104 was quantifiable only in plasma ($AUC_{0\text{-}t}$ = 0.65 nmol hour/ml), while no DRP-104 was observed in tumor or intestinal tissue. DRP-104 delivered a 6-fold higher exposure of DON to the tumor as measured by area under the curve ($AUC_{0\text{-}t}$ = 4.13 ± 0.59 nmol hour/g) versus plasma (0.67 ± 0.03 nmol hour/ml) and 11-fold higher exposure versus intestinal tissue (0.36 ± 0.13 nmol hour/g). Quantitation of the inactive M1 metabolite revealed highest levels in the intestinal tissue (3.2 ± 0.85 nmol hour/g), with 6- and 15-fold lower concentrations in plasma (0.56 ± 0.09 nmol hour/ml) and tumor (0.22 ± 0.0.2 nmol hour/ml), respectively (Fig. 2G). These data show that DRP-104 administration leads to a preferential delivery of active DON to tumor and inactive M1 metabolite to GI tissues.

Following the PK studies, we next evaluated target engagement in the tumor using two different biomarkers. First, we quantified tumor formylglycinamide ribonucleotide (FGAR), an intermediate in the de novo purine synthesis pathway known to be altered by DON (*14*, *45*) using our validated LC-MS method (*44*). Second, we quantified inhibition of GLS-1 activity in the tumor using our radiolabel-based enzymatic assay (*41*). Briefly, DON or DRP-104 was administered subcutaneously, and tumor samples were collected 1 hour after dose. FGAR was found to be significantly increased >80-fold in the tumors of both DON- and DRP-104–treated mice compared to the vehicle-treated group (fig. S6A). Similarly, DON- and DRP-104–treated mice showed significant inhibition of tumor

GLS-1 activity compared to the vehicle-treated group (fig. S6B). Tumor levels of DON were similar in the DON- and DRP-104–treated mice, exhibiting pharmacokinetic/pharmacodynamic (PK/PD) correlation (fig. S6C).

To ensure that its tumor-targeting profile was not specific to EL4 tumors, the PK of DRP-104 was also assessed in three other syngeneic tumors including MC38 (colon cancer), E0771 (breast cancer), and 3LL (Lewis lung carcinoma), with comparable results (fig. S7, A to D). We also compared the PK of DRP-104 to a previously reported DON prodrug called JHU-083. DRP-104 was found to be superior to JHU-083, showing a >2.5-fold improved tumor/plasma and >3-fold improved tumor/GI tissue partitioning ratio (fig. S8, A and B). These in vivo results concurred with the in vitro metabolism of DRP-104 (Fig. 2 and fig. S2) and confirmed the superior preferential tumor DON delivery of DRP-104 versus JHU-083.

DRP-104 is bioactivated in the tumor by serine proteases; DRP-104 is bioinactivated in GI tissue by carboxylesterases

To elucidate the mechanism of preferential DON release in tumor versus GI tissue, stability analysis of DRP-104 was evaluated under various conditions in both EL4 tumor homogenates and mouse intestinal tissue homogenates. First, the stability of DRP-104 was evaluated in mouse tumor homogenates with and without a cocktail of multiple classes of protease inhibitors. DRP-104 was unstable when incubated in tumor homogenate (0% remaining at 60 min); in contrast, DRP-104 showed complete stability in tumor homogenate when coincubated with the protease inhibitor cocktail. Next, the stability of DRP-104 was evaluated in the presence of individual components of the cocktail, including Pefabloc, phenylmethylsulfonyl fluoride (PMSF), aprotinin, bestatin, E64, leupeptin, and pepstatin A. Of the seven protease inhibitors tested, only the serine protease inhibitor Pefabloc and the dual serine protease and esterase inhibitor PMSF attenuated DRP-104 tumor metabolism. The other classes of inhibitors (aminopeptidase, aspartyl peptidase, cysteine peptidase, serine peptidase, and threonine peptidase inhibitors) had no effect (Fig. 3A). In contrast, when these same seven protease inhibitors were tested on intestinal tissue homogenate, Pefabloc had little effect on DRP-104 metabolism, while PMSF showed almost complete inhibition of DRP-104 metabolism, suggesting that the intestinal metabolism was primarily due to esterase activity (Fig. 3B).

To delineate the metabolic effects of Pefabloc and PMSF in tumor and intestinal tissue, detailed metabolite identification (MET-ID) studies were performed. As depicted in Fig. 3 (C and D), both DON and M1 metabolite were found in the tumor, but only the M1 metabolite was observed in the GI tissue. We then tested the effect of dichlorvos, a specific esterase inhibitor, on DRP-104 intestinal metabolism. We showed that dichlorvos almost completely inhibited DRP-104 metabolism in the intestinal matrices, further confirming the involvement of esterase activity. In contrast, dichlorvos had minimal effect on the metabolism of DRP-104 in tumor homogenate (Fig. 3, E and F). Last, we confirmed these findings using recombinant CES1 enzyme and demonstrated that CES1 was capable of metabolizing DRP-104 to M1 metabolite in the mouse intestinal tissue (fig. S9). We also showed that M1 metabolite was stable in intestinal tissue with minimal DON release (fig. S4). These data, combined with the stability and in vivo PK data, confirm the distinct metabolic pathways for DRP-104 in tumor versus GI tissue (Fig. 3G). In tumor, DRP-104 underwent amide hydrolysis to form DON isopropyl ester, which then spontaneously hydrolyzed to release DON. In contrast, in the intestinal matrix, de-esterification of the isopropyl ester to form the stable and inactive M1 metabolite was the major metabolic pathway.

DRP-104 was similarly efficacious to DON in inhibiting tumor growth but with a marked reduction in toxicity

DRP-104 and DON (1 mg/kg DON equivalent, intravenously) were administered 5 days per week for 2 weeks to C57BL/6/CES1$^{-/-}$ mice bearing EL4 tumors. Both DRP-104 and DON caused complete regression of the tumor (Fig. 4A). However, DON administration resulted in a substantial 20 to 30% body weight reduction, while DRP-104–treated mice maintained their body weight throughout the study duration (Fig. 4B). While they had minimal tumor burden, most DON-treated mice required euthanasia due to overt toxicity and/or weight loss. In contrast, no deaths were observed in the DRP-104 treatment group (Fig. 4C). At the end of treatment, remaining mice were sacrificed and evaluated for toxicity by complete blood count (CBC) (table S2) and GI histology (Fig. 4D). CBC analysis was in the normal range for all groups except for a modest reduction in white cell counts in the DON-treated mice (0.93 ± 0.18 versus normal range of 1.06 to 56.08 K/μl). These results suggested limited systemic toxicity in either treatment group. In contrast, the GI histology was markedly different between the treatment groups. Vehicle-treated mice maintained a normal, intact mucosal layer with organized crypts and abundant goblet cells. However, DON-treated mice showed severe GI toxicity with widespread ulceration of the mucosal layer, abundant neutrophil and lymphocyte infiltrates, and prominent bacterial mats. DRP-104–treated mice, while not normal, had improvement in all these parameters (Fig. 4D), which was further confirmed by blinded histopathological scoring of inflammation and architecture (fig. S10).

In addition to comparison with DON intravenous administration, DRP-104 was also evaluated at multiple systemic doses (0.1, 0.3, and 1 mg/kg DON equivalent, subcutaneously, 5 days per week) to assess the minimum effective dose with assessment of toxicity in tandem. DRP-104 resulted in a dose-dependent inhibition of tumor growth, with significant tumor regression observed at the highest dose (Fig. 5A). No overt signs of toxicity were observed at any of the doses, with minimal effects on body weight throughout the study duration (Fig. 5B). Further, at the end of the treatment, all cohorts were sacrificed and evaluated for GI histopathology changes (Fig. 5C and fig. S10). The GI morphology looked normal at the 0.1 and 0.3 mg/kg doses; however, at 1 mg/kg, mild lymphocytic infiltration was observed (Fig. 5C).

Global metabolomic/flux analyses showed prominent DRP-104 effects on multiple pathways

To investigate the metabolic changes associated with DRP-104 therapy in EL4 tumors, global metabolic profiling was performed following DRP-104 treatment (0.3 mg/kg DON equivalent dosed subcutaneously for 5 days) versus vehicle controls. With respect to polar metabolites, DRP-104 administration led to a metabolic shift as determined by principal components analysis (Fig. 6A). Eighty-eight metabolites showed absolute fold change of ≥ 2 ($P \leq 0.1$) (Fig. 6B and table S3). Analysis of the top affected metabolites revealed that DRP-104 caused metabolic changes in multiple pathways, including effects on amino acids, nucleotides, and carbohydrates/TCA cycle intermediates (Fig. 6C). DRP-104 treatment significantly affected glutamine-derived intermediates in the TCA cycle, decreasing metabolites

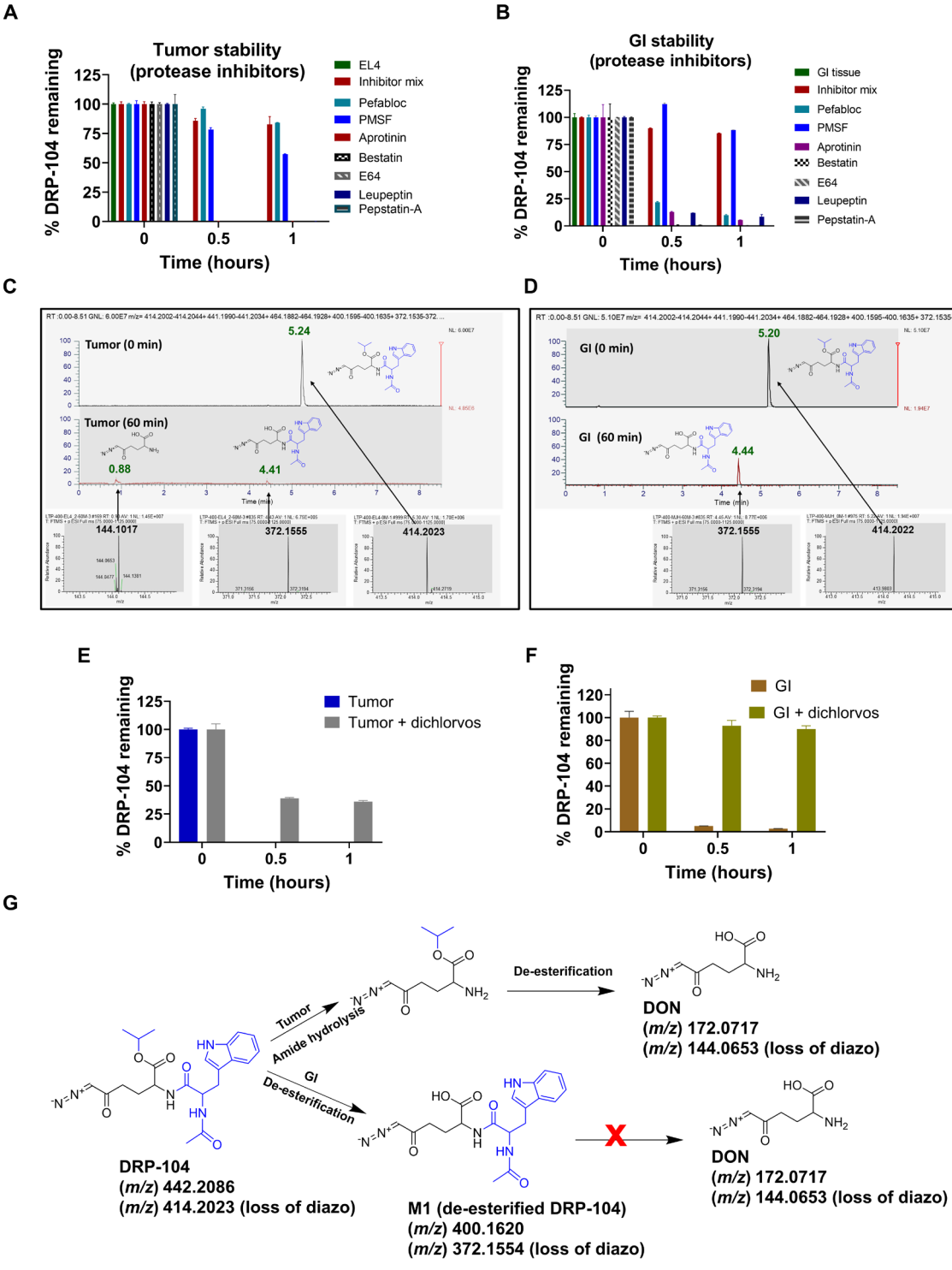

Fig. 3. Mechanism of DRP-104 bioactivation in tumor versus GI. Stability of DRP-104 in (**A**) tumor homogenate (**B**) versus GI tissues in the presence of protease inhibitor cocktail and its individual components. The protease inhibitor cocktail inhibited metabolism of DRP-104 in both tumor and GI tissue. Of the individual components, only Pefabloc (serine protease inhibitor) and PMSF (dual esterase and serine protease inhibitor) showed inhibition of DRP-104 metabolism in tumor. PMSF also showed inhibition of DRP-104 metabolism in GI. MET-ID studies in (**C**) tumor and (**D**) GI tissue following 60-min incubation. At time 0, $m/z = 414.2023$ peak was observed (retention time = 5.2 min) corresponding to the presence of DRP-104. In tumor, DON [$m/z = 144.1017$; retention time (RT) = 0.88 min] and M1 ($m/z = 372.1554$; RT = 4.4 min) were observed. In contrast, only M1 ($m/z = 372.1554$; RT = 4.4 min) was observed in GI. Specific esterase inhibitor dichlorvos had limited effect in (**E**) tumor but (**F**) inhibited DRP-104 instability in GI. (**G**) Distinct pathways for DRP-104 bioactivation in tumor versus GI.

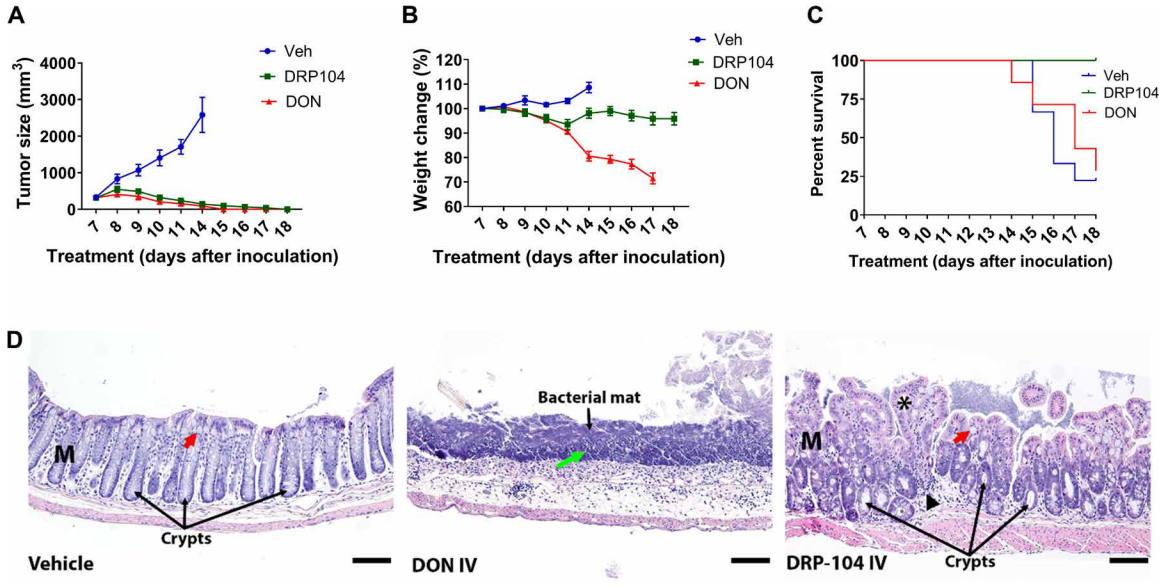

Fig. 4. Comparison of the efficacy and toxicity of equimolar DON and DRP-104 in EL4 tumor-bearing C57BL/6/CES1$^{-/-}$ mice. Equimolar doses of DRP-104 and DON (1 mg/kg equivalent, intravenously, dosed 5 days/week for 2 weeks) were administered to mice bearing flank EL4 tumors. (**A**) Both DON and DRP-104 treatment resulted in complete tumor regression. (**B**) DON caused substantial body weight loss, while DRP-104–treated mice maintained their body weight throughout the study. (**C**) All vehicle-treated mice required euthanasia based on IACUC tumor volume guidelines. Most (63%) of the DON-treated mice required euthanasia based on IACUC weight loss guidelines. In contrast, no deaths were observed in the DRP-104 treatment group. (**D**) Vehicle-treated mice had an intact mucosal layer (M) with organized crypts and abundant goblet cells (red arrow). DON-treated mice exhibited severe and widespread ulcerations of the mucosal layer with abundant neutrophil and lymphocyte localization (green arrow) adjacent to the bacterial mats. DRP-104–treated mice had less severe GI changes with a maintained mucosal layer (M) but with some reduction of goblet cells (red arrow), epithelial hyperplasia (asterisk), lymphocytic infiltrations, and edema of the lamina propria (black arrowhead), as well as general disorganization and dilation of the crypts. Scale bars, 100 μm. Original magnification, ×20.

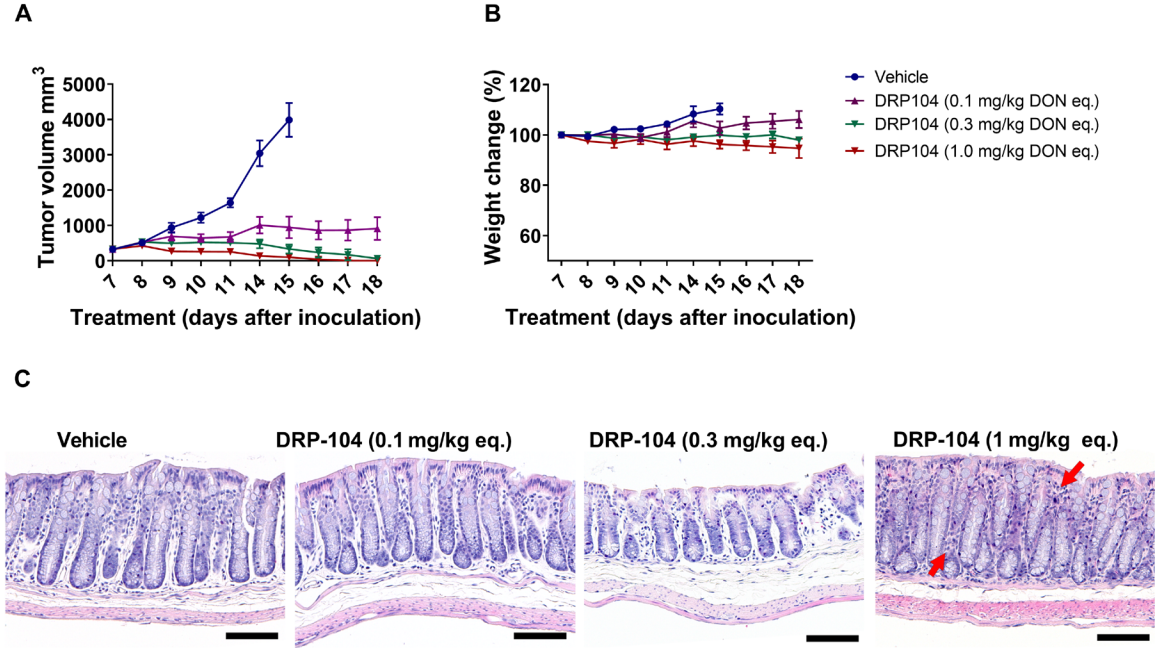

Fig. 5. Dose-dependent efficacy and toxicity of subcutaneously administered DRP-104 in EL4 tumor-bearing C57BL/6/CES1$^{-/-}$ mice. (**A**) DRP-104 administration (0.1, 0.3, and 1 mg/kg DON equivalent delivered subcutaneously 5 days per week) resulted in a dose-dependent reduction in tumor growth with complete tumor regression at the higher two doses. (**B**) Minimal effects on body weight were observed at all doses. (**C**) Subcutaneous administration of DRP-104 had no adverse effect on GI histopathology at the lower doses; at the highest dose, mild lymphocytic infiltration (indicated by red arrows) was observed. Scale bars, 100 μm. Original magnification, ×20.

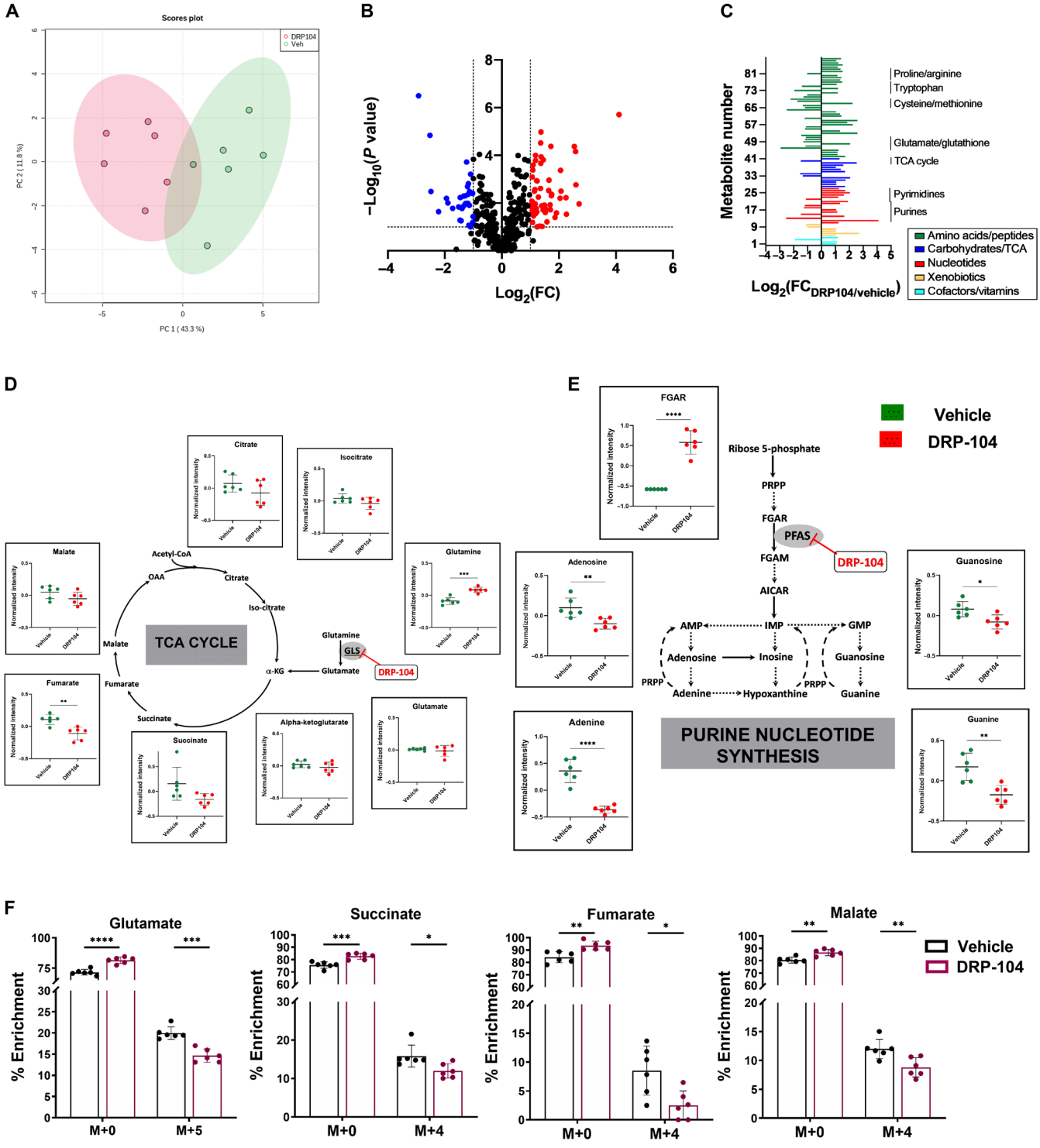

Fig. 6. Metabolomic analysis of DRP-104–treated tumors. (**A**) Principal components analysis of metabolomics datasets of the EL4 tumors in the vehicle- versus DRP-104–treated mice (green = vehicle; red = DRP-104). (**B**) Volcano plot of metabolites identified from EL4 tumors treated with DRP-104 or vehicle. *X* axis is $\log_2$ (fold change DRP-104/vehicle); *y* axis is $-\log_{10}$ (*P* value). Metabolites with $\log_2$ fold change ≤ −1 and $-\log_{10}$ (*P* value) ≥ 1 are blue. Metabolites with $\log_2$ fold change ≥ 1 and $-\log_{10}$ (*P* value) ≥ 1 are red. All other metabolites are shown in black. (**C**) Individual significant ($P < 0.1$) metabolites ($n = 88$) from DRP-104 versus vehicle-treated EL4 tumors categorized by metabolic superpathways. Subpathways highlighted by black bars and text. *X* axis is $\log_2$ (fold change DRP-104/vehicle). *Y* axis is list of metabolites. (**D**) Major TCA cycle components affected by DRP-104 treatment. (**E**) Major purine nucleotide synthesis components affected by DRP-104 treatment. (*$P \leq 0.05$, **$P \leq 0.01$, ***$P \leq 0.001$, and ****$P \leq 0.0001$ based on unpaired *t* test.) (**F**) $^{13}C_5$-glutamine flux analysis of DRP-104–treated tumors. Emphasis is on isotopologue enrichment of TCA cycle intermediates such as glutamate, succinate, fumarate, and malate. *$P \leq 0.05$, **$P \leq 0.01$, ***$P \leq 0.001$, and ****$P \leq 0.0001$, based on multiple *t* tests.

such as succinate, fumarate, and malate (Fig. 6D). Metabolomic profiling also demonstrated prominent effects on purine metabolism (Fig. 6E) as well as tryptophan metabolism (fig. S11). FGAR, a substrate for PFAS in the de novo purine synthesis pathway, was prominently increased with DRP-104 treatment, and products of purine synthesis, including adenine and guanine, were decreased upon DRP-104 treatment (Fig. 6E). Last, consistent with its inhibition of glutamine-using enzymes, DRP-104–treated mice showed increased glutamine levels (Fig. 6D). Together, these findings highlight the broad metabolic effects of DRP-104 on tumors.

Given the prominent effects of DRP-104 on TCA cycle intermediates, we further examined these effects using $^{13}C_5$-glutamine flux analysis in mice bearing EL4 tumors (Fig. 6F). Briefly, mice were treated with vehicle or DRP-104 (0.3 mg/kg DON equivalent, subcutaneously) for 3 days. On day 4, mice received DRP-104, followed by tail vein injections of $^{13}C_5$-glutamine, and tumors were harvested 1 hour later for metabolite analysis. We observed that of the total glutamate pool in control (vehicle-treated) tumors, 19.99% was from the M+5 isotopologue, suggesting that $^{13}C_5$-glutamine was taken up by tumors and underwent metabolism in the time frame of the experiment. DRP-104–treated tumors had 14.66% of the total glutamate pool from the M+5 isotopologue; this was a significant difference versus control tumors, suggesting that glutamine-dependent metabolism was inhibited in DRP-104–treated tumors. We also observed a significant decrease in the enrichment of the M+4 isotopologue in total pool of succinate, fumarate, and malate in DRP-104–treated tumors compared to control tumors (Fig. 6F). These data suggest that DRP-104 inhibited the influx of glutamine-derived glutamate into the TCA cycle.

DRP-104 enhanced anti-PD-1 efficacy; DRP-104 effect was CD8$^+$ T cell dependent and resulted in immunological memory

DRP-104 (0.3 mg/kg DON equivalent, subcutaneously, 5 days per week, four cycles), anti-PD-1 (100 μg, intraperitoneally, four doses), or the combination thereof was administered to MC38 tumor-bearing C57BL/6/CES1$^{-/-}$ mice. DRP-104 and anti-PD-1 monotherapies resulted in significant MC38 tumor growth inhibition. However, the combination of DRP-104 with anti-PD-1 therapy showed a significant improvement in efficacy compared to the monotherapies alone (Fig. 7A). No overt toxicities or body weight changes were observed throughout the study duration (Fig. 7B and fig. S13). In addition to tumor growth inhibition, both DRP-104 and anti-PD-1 monotherapy resulted in enhanced survival compared to vehicle. Moreover, the combination further improved survival versus the monotherapies (Fig. 7C). Drug treatment was stopped after 28 days (dosing 5 days per week for four cycles), and tumor rebound was assessed. Tumor rebound with the combination therapy (1 of 10) was superior when compared to either anti-PD-1 or DRP-104 monotherapy (4 of 10 for both) (Fig. 7D). To study the possible immunologic memory effects of DRP-104, mice that had initially been cured with 2 weeks of DRP-104 monotherapy were rechallenged with an equal burden of MC38 tumor in the opposite flank 60 days after the last dose of therapy. Mice received no further treatment. In all cases, mice that had previously been cured with DRP-104 monotherapy completely rejected tumor rechallenge (Fig. 7E), suggesting that immunologic memory had been established through glutamine blockade.

We hypothesized that the immune response triggered by DRP-104 was CD8$^+$ T cell–mediated. To test this, we used CD8$^+$ T cell–depleting antibodies in MC38-bearing C57BL/6/CES1$^{-/-}$ mice and compared the effects of DRP-104 after CD8$^+$ T cell depletion versus isotype-treated controls. We found that the efficacy of DRP-104 was completely dependent on CD8$^+$ T cell response (Fig. 8, A and B). Flow cytometric analysis was performed on tumor-infiltrating lymphocytes (TILs) in C57BL/6/CES1$^{-/-}$ mice bearing ovalbumin (OVA)–expressing MC38 tumors (MC38OVA) treated with vehicle or DRP-104. By using an OVA-expressing tumor system, we were able to track antigen-specific T cell responses using tetramer staining. Consistent with our previous reports (*18*), these studies revealed phenotypic changes in the infiltrating CD8$^+$ T cell population consistent with a central memory-like (CD62L$^+$CD44$^+$) phenotype in DRP-104–treated mice (Fig. 8C). Compared with DRP-104–treated mice, CD8$^+$ TILs from vehicle-treated control mice showed increased coexpression of inhibitory pathways (PD-1$^+$LAG3$^+$) and transcription factor expression patterns (TOX$^+$TCF1^{LO}) characteristic of a terminally exhausted phenotype (Fig. 8, D and E). Antigen-specific CD8$^+$ T cells were enriched in the TIL from DRP-104–treated mice (Fig. 8F) and displayed suppressed exhaustion markers and increased TCF1 expression characteristic of a robust, durable antitumor response and stem-like phenotype (Fig. 8G). Tumor-infiltrating CD8$^+$ T cells in DRP-104–treated mice showed increased expression of activation markers (CD44, CD69, and T-bet), as well as markers of stem-like memory phenotype (TCF1, CD28, BCL6, EOMES, CD122, CD127, and CD62L) (Fig. 8H). These phenotypic characteristics seemed to be specific to infiltrating CD8$^+$ T cells as they were not detected in the draining lymph nodes of treated mice (fig. S12, A and B). These studies demonstrate that the antitumor response triggered by DRP-104 is strongly dependent on the ability of the drug to enhance the endogenous immune response through a CD8-mediated mechanism.

DISCUSSION

Glutamine is a critical element of cancer metabolism driving many cancer cells to "glutamine addiction" (*46*–*48*). Our recent studies showed that antagonizing glutamine utilization with DON induces tumor regression by a dual mechanism, including both starving cancer cells of glutamine to feed anabolism while simultaneously conditioning the tumor microenvironment to enhance effector T cell function (*18*), making glutamine starvation a particularly attractive therapy. Unfortunately, glutamine antagonists such as DON have not been developed clinically mainly due to dose-limiting GI toxicities. Here, we report the design of a dual promoeity glutamine antagonist prodrug that is bioactivated in the tumor to release DON (target site) while simultaneously bioinactivated to an inert metabolite in GI tissues (toxicity site) (Fig. 9). This differential metabolism of DRP-104 results in a prodigious 11-fold higher DON exposure in the tumor versus the GI tract, leading to robust anticancer activity with minimal GI toxicity. This novel prodrug design is permitting the reentry of this robust metabolic inhibitor into clinical trials.

The tolerability of chemotherapy, in part, depends on the selective vulnerability of tumor cells relative to normal tissue. In the case of DON, with its broad metabolic effects, we hypothesized that a targeted drug delivery mechanism would be needed to facilitate high DON exposure in cancer cells while curtailing its systemic exposure, especially to GI tissues, to improve its therapeutic index (*49*). One popular targeting strategy is to develop nontoxic prodrug forms of anticancer agents that can be bioactivated by the endogenous

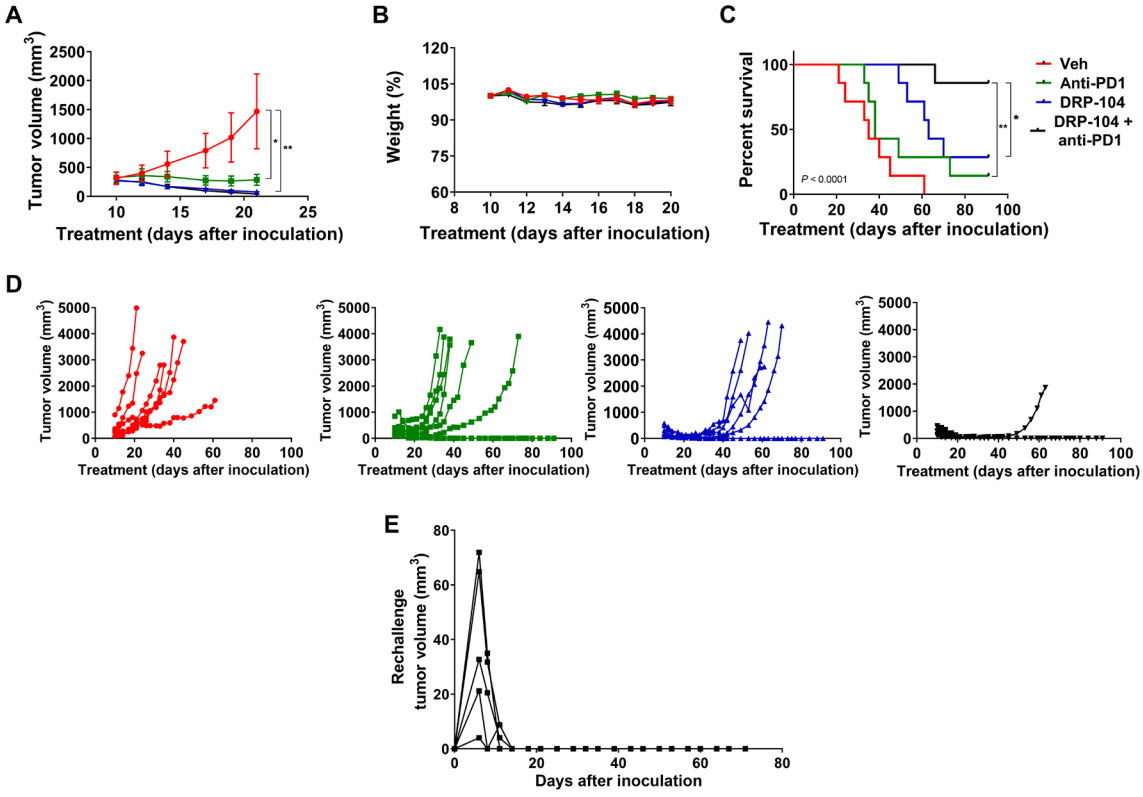

Fig. 7. DRP-104 enhances anti-PD-1 efficacy in MC38 tumor-bearing C57BL/6/CES1$^{-/-}$ mice. DRP-104 (0.3 mg/kg DON equivalent, subcutaneously, 5 days per week, four cycles), anti-PD-1 (100 μg, intraperitoneally, four doses), or the combination was administered to MC38 tumor-bearing C57BL/6/CES1$^{-/-}$ mice from 10 to 36 days after inoculation, after which all drug therapy was discontinued. (**A**) DRP-104 and anti-PD-1 monotherapy resulted in significant tumor growth inhibition as compared to vehicle ($P < 0.05$ and $P < 0.01$, respectively), as did the DRP-104 and anti-PD-1 therapy combination ($P < 0.01$). Inhibition of tumor growth is shown until the first sacrifice. (**B**) Administration of DRP-104, anti-PD-1, and the combination had no substantial effect on body weight throughout the experiment. Data are shown until the first sacrifice (data for the entire experiment are shown in fig. S13). (**C**) Both DRP-104 and anti-PD-1 monotherapy resulted in enhanced survival as compared to vehicle ($P < 0.001$). When DRP-104 was combined with anti-PD-1 therapy, the combination improved survival as compared to anti-PD-1 ($P < 0.01$) or DRP-104 monotherapy ($P < 0.05$). (**D**) Spider plots of individual mice data treated with either vehicle, anti-PD-1, DRP-104, or anti-PD-1 + DRP-104 show a significant reduction in tumor rebound in the anti-PD-1 + DRP-104 combination–treated mice. (**E**) Mice initially cured with 2 weeks of DRP-104 monotherapy (0.1 and 0.3 mg/kg DON equivalent dose) were challenged with MC38 cells on the opposing flank 60 days after the last dose of therapy. These mice showed complete rejection of tumor; spider plots of tumor volume are shown.

enzymes overexpressed in tumors (*50*–*55*). In the past decade, five anticancer prodrugs have been approved by the U.S. Food and Drug Administration including ixazomib citrate, aldoxorubicin, evofosfamide, abiraterone acetate, and romidepsin (*56*, *57*). Using a similar, yet distinct strategy, we synthesized a series of DON prodrugs by installing dual promoieties (P1 to P8; fig. S1) that can be dislodged by the enriched milieu of esterase and protease enzymes in tumors (*54*, *58*–*62*). Initial in vitro characterization revealed DRP-104 as the most promising prodrug with optimal stability profile and tumor partitioning results (fig. S2), and thus, it was selected for further evaluation.

DRP-104 was stable when incubated in plasma and GI tissue, releasing negligible DON at these nontumor, off-target sites (Fig. 2, A to C). In contrast, DRP-104 was markedly metabolized to DON in tumor cells, resulting in similar cytotoxic effect (fig. S5). In vivo, when administered to tumored mice, DRP-104 yielded a robust 11-fold higher DON exposure in the tumor versus GI tissue (Fig. 2, E to G). This magnitude of preferential, on-target delivery of a chemotherapeutic agent is exceptional and is superior to many clinically available tumor-targeted prodrugs. For example, the oral fluoropyrimidine prodrug capecitabine is preferentially converted to 5-fluorouracil in target tumor tissue (by three-step activation), with the average concentration being 3.2-fold higher in tumor than in adjacent healthy tissue (*63*). CPT-11 (irinotecan), a prodrug of camptothecin bioactivated by carboxylesterases, shows similar plasma and tumor levels of the active drug (*64*). Other examples of tumor targeting drugs are combretastatin A4 phosphate (CA4P), exhibiting two- to threefold higher tumor versus plasma delivery (*65*), as well as folic acid– and Evans blue–conjugated paclitaxel prodrug with prolonged blood circulation and enhanced two- to threefold drug accumulation in tumor versus plasma (*66*).

In addition to the PK evaluation in the EL4 lymphoma model, we used two biomarker strategies to confirm target engagement in the tumor (fig. S6). DRP-104 administration resulted in a significant increase in FGAR (>80-fold), an intermediate in the de novo purine synthesis pathway known to be altered by DON (*45*), as well as significant inhibition of GLS-1 activity, an enzyme that catalyzes the conversion of glutamine to glutamate (*41*, *67*). Moreover,

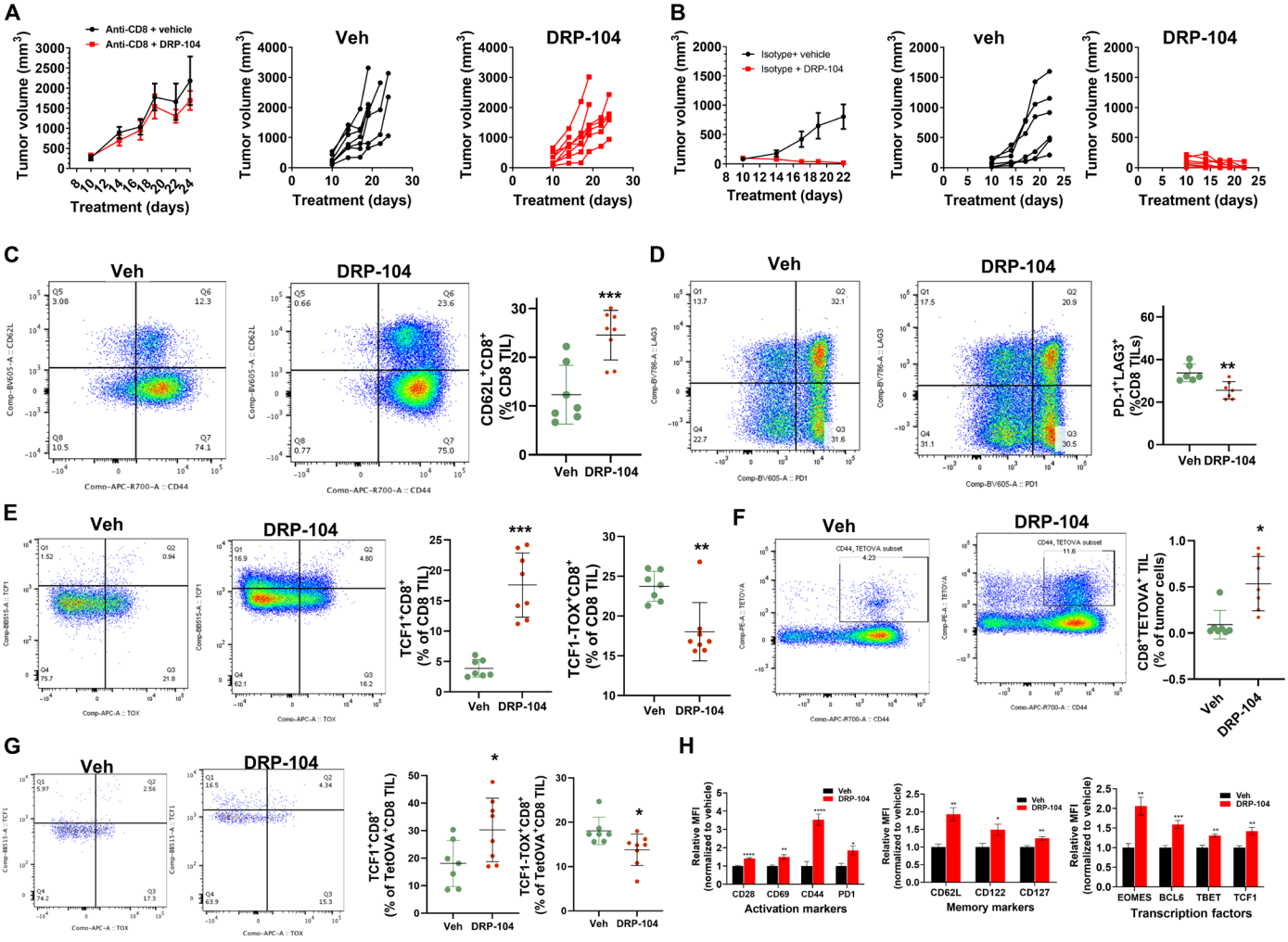

Fig. 8. DRP-104 causes CD8$^+$ T cell–dependent tumor regression secondary to memory stem-like conditioning of infiltrating CD8$^+$ T cells. (**A**) MC38-bearing CES1$^{-/-}$ mice treated with DRP-104 (0.3 mg/kg DON equivalent, subcutaneously, 5 days per week) after depletion of CD8$^+$ T cells; spider plots of individual mice data from vehicle or DRP-104. (**B**) OVA-expressing MC38-bearing CES1$^{-/-}$ mice treated with vehicle or DRP-104; tumor growth curves of individual mice are depicted from vehicle and DRP-104 groups. Representative flow cytometry plots (left) and data charts (right) from CD8$^+$ TIL showing (**C**) CD44 and CD62L, (**D**) PD-1 and LAG3, and (**E**) TCF1 and TOX defined subsets. (**F**) Flow cytometry showing antigen-specific tetramer-positive CD8$^+$ TIL and (**G**) TCF1 and TOX defined subsets within tetramer-OVA–positive population. (**H**) Relative mean fluorescence intensity data plots for activation markers, memory/stem cell markers, and transcription factors in CD8 TILs. *$P < 0.05$, **$P < 0.01$, ***$P < 0.001$, and ****$P < 0.0001$, based on *t* test.

DRP-104 PK was also confirmed in three other tumor types, where it showed similar preferential tumor delivery of DON (fig. S7), substantiating broad specificity to tumor-enriched enzymes.

In vitro stability studies using protease inhibitors and recombinant enzymes followed by extensive MET-ID studies were used to elucidate the mechanism of DRP-104 metabolism. In GI tissue homogenate, DRP-104 primarily exhibited de-esterification of its isopropyl ester by carboxylesterases, yielding an inactive metabolite M1 that was resistant to further hydrolysis (Fig. 3, D and G, and fig. S4). This was confirmed using recombinant human CES1 enzyme (fig. S9). In contrast, in tumor homogenate, while the de-esterified metabolite existed, a second prominent pathway involving both de-esterification and hydrolysis of the *N*-promoiety by a serine protease was observed, resulting in the release of active DON (Fig. 3, C and G). Note that these studies were systematically designed to evaluate the stability and PK of DRP-104 in C57BL/6/CES1$^{-/-}$ mouse model recapitulating human prodrug metabolism; however, expression and localization of enzymes can vary among different species (*68*, *69*). For example, CES1 enzyme is highly abundant in mouse intestine, but it is not expressed in human intestine, which mostly expresses CES2 (*69*). Such interspecies differences may have implications in prodrug bioactivation, like that reported for other prodrugs of approved cytotoxic agents (*56*, *63*, *64*, *70*).

Efficacy evaluation at equimolar doses revealed that both DRP-104 and DON were equally efficacious in causing almost complete tumor regressions; however, most (63%) of the DON-treated mice required euthanasia based on Institutional Animal Care and Use Committee (IACUC) weight loss guidelines; in contrast, the DRP-104 mice maintained their body weight throughout the study. On necropsy, all DON mice showed extreme and widespread GI histological abnormalities, whereas DRP-104–treated mice exhibited minimal GI effects (Fig. 4 and fig. S10).

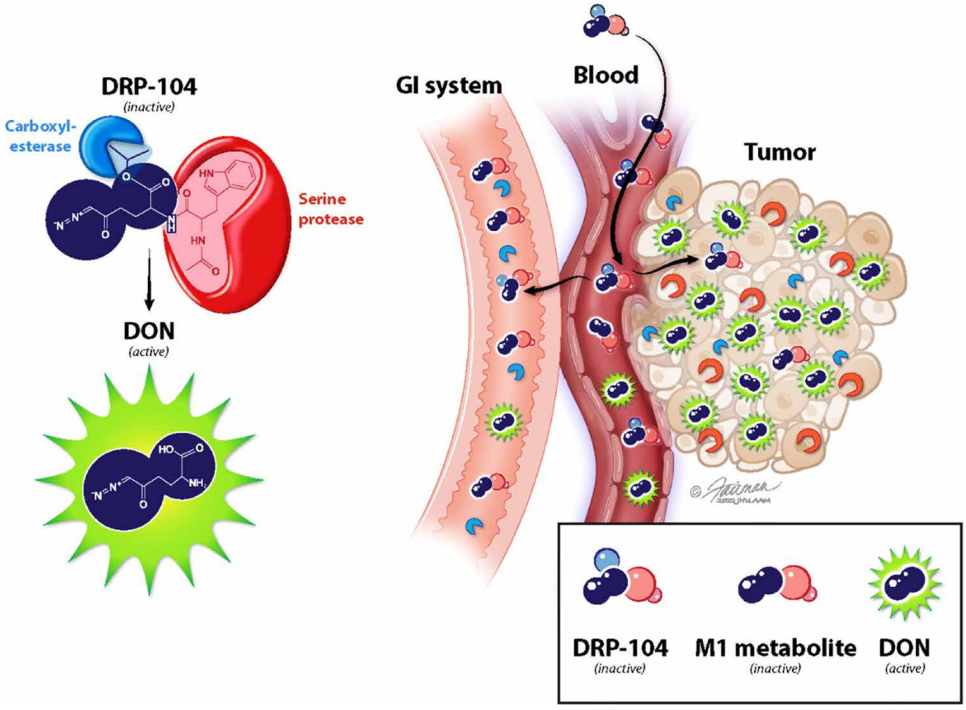

Fig. 9. Schematic for DRP-104's bioactivation to DON in tumor and bioinactivation to the inactive M1 metabolite in GI tissues following systemic administration. (Illustration by Jennifer E. Fairman, CMI, FAMI 2022 JHU AAM.)

To elucidate the mechanistic role of DRP-104 on cancer cell metabolism, global metabolomics profiling was conducted in tumors. DRP-104 treatment led to the perturbation of multiple metabolic pathways (Fig. 6, A to E) including amino acid, nucleotide, and TCA cycle metabolites. It affected downstream glutamine-dependent metabolites in the TCA cycle and inhibited purine synthesis, resulting in a robust accumulation of FGAR, an intermediate in the de novo purine synthesis pathway. The increase in FGAR is attributed to the inhibition of PFAS, the enzyme that catalyzes the glutamine- and adenosine triphosphate (ATP)–dependent amidation of FGAR to formylglycinamidine ribonucleotide (*44*, *45*). In further support, the levels of purine bases (e.g., adenine) and nucleosides (e.g., 1-methyladenosine) also declined with DRP-104. DRP-104 treatment affected amino acids including those in the tryptophan/kynurenine pathway; for example, 3-hydroxykynurenine, a product of an indoleamine 2,3-dioxygenase (IDO)–dependent pathway, was decreased (fig. S11). This supports earlier findings that glutamine antagonism affects IDO metabolism, and this mechanism is relevant to its efficacy when combined with immunotherapy (*71*). In addition, several metabolites in proline metabolism and dipeptides in collagen turnover (table S3) (e.g., leucyl hydroxyproline) were affected by DRP-104 treatment, consistent with a previous report of DON affecting collagen metabolism and extracellular matrix production (*72*). Last, because untargeted metabolomics demonstrated significant effects of DRP-104 on multiple TCA cycle intermediates, we confirmed these observations using in vivo metabolic flux analysis with isotopically labeled $^{13}C_5$-glutamine. Mice treated with DRP-104 exhibited inhibition in the enrichment of M+5 glutamate and M+4 malate, fumarate, and succinate isotopologues compared to vehicle-treated mice (Fig. 6F). Together, these metabolomic analyses confirmed perturbations of relevant glutamine-dependent pathways in DRP-104–treated tumors, similar to that reported previously with DON (*18*, *44*). Further evaluation of prominently affected metabolites, particularly those that are plasma measurable or could be assessed by noninvasive techniques, could provide directions for development of efficacy or target engagement biomarkers.

Given our recent observations that glutamine inhibition stimulates antitumor immune response, we also assessed the efficacy of DRP-104 in combination with anti-PD-1 immunotherapy. We had observed previously that glutamine antagonism and PD-1 checkpoint immunotherapy led to a robust enhancement of T cell efficacy in tumor-bearing mice when compared with anti-PD-1 therapy alone (*18*). Specifically, we showed that glutamine blockade, in addition to disrupting tumor metabolic programs, can condition antitumor $CD8^+$ T cells toward a more effective and long-lived phenotype. These differing effects on cancer cells and corresponding $CD8^+$ T cells were correlated with a higher degree of metabolic flexibility of $CD8^+$ T cells compared with tumor cells. This was particularly evident in the ability of $CD8^+$ T cells (unlike most cancer cells) to engage in catabolism of acetate as an alternative fuel source for TCA cycle function in the setting of glutamine blockade. Whereas cancer cells are profoundly disabled through glutamine blockade, with suppressed levels of both aerobic glycolysis and oxidative phosphorylation, $CD8^+$ T cells can compensate and thrive by up-regulating acetate metabolism (*18*). As such, glutamine blockade is able to drive a wedge between the metabolic fitness of cancer cells and responding antitumor $CD8^+$ T cells. These effects are dependent on broadly inhibiting glutamine metabolic programs and, as such, are not observed during targeted glutaminase inhibition with agents such as CB-839. In accord with these findings, our studies demonstrated that DRP-104 robustly synergized with anti-PD-1 checkpoint blockade and led to significant improvement in tumor growth suppression and survival (Fig. 7).

Furthermore, we showed that tumor responses during DRP-104 monotherapy were $CD8^+$ T cell dependent, and infiltrating T cells demonstrated phenotypic changes consistent with a long-lived, stem-like phenotype characteristic of a durable antitumor response (Fig. 8). These changes established a robust immunologic memory in DRP-104–treated mice, demonstrated by complete tumor rejection upon rechallenge (Fig. 7E).

In summary, we report the discovery of a first-in-class prodrug that exhibits divergent metabolism in target versus toxicity tissue sites, leading to a well-tolerated glutamine antagonist with robust anticancer efficacy. This novel approach of creating prodrugs that simultaneously are enriched in target tissues and decreased in tissues susceptible to toxicity has potentially broad application in altering the therapeutic index of active yet otherwise toxic chemotherapies.

MATERIALS AND METHODS

Metabolic stability studies

Human and mouse plasma (WT) were purchased from Innovative Research (Novi, MI). S9 fraction (intestine) was purchased from XenoTech LLC (Kansas City, KS). Recombinant CES1 enzyme was purchased from Sigma-Aldrich. Commercially available LC-MS–grade solvents were purchased from Thermo Fisher Scientific (Fair Lawn, NJ). The in vitro plasma (WT and C57BL/6/$CES1^{-/-}$ mouse, and human), S9 fraction (intestine), and GI tissue homogenate (C57BL/6/$CES1^{-/-}$ mouse) stability assays were performed following our previously reported methods (*73*). The stability of DRP-104 was monitored by spiking DRP-104 at a concentration of 20 μM in 1 ml of plasma. Stability in intestinal S9 fractions was assessed at 10 μM with a final protein concentration of 1 mg/ml. For the C57BL/6/$CES1^{-/-}$ mice GI homogenate studies, tissues were diluted [10-fold in 0.1 M (pH 7.4) potassium phosphate buffer] and homogenized using a probe sonicator. DRP-104 was incubated at a concentration of 20 μM. For the recombinant CES1 enzyme stability, DRP-104 was incubated at 20 μM in tris buffer (50 mM, pH 7.5) with an enzyme concentration of 10 μg/ml. Spiked samples (in triplicate) were incubated in an orbital shaker at 37°C for 1 hour (up to 3 hours for CES1 enzyme) and quenched with three volumes of acetonitrile containing internal standard (IS; losartan: 0.5 μM). Samples were vortex-mixed for 30 s and centrifuged at 10,000*g* for 10 min at 4°C. The disappearance of DRP-104 over time was monitored using LC-MS/MS. Briefly, samples were analyzed on a Thermo Fisher Scientific Accela ultrahigh-performance liquid chromatography (UPLC) system coupled to Accela open autosampler with an Agilent Eclipse Plus column (100 mm × 2.1 mm internal diameter.; maintained at ambient temperature) packed with a 1.8-μm C18 stationary phase. The autosampler was temperature-controlled and operated at 10°C. The mobile phase used for chromatographic separation consisted of acetonitrile and water, both containing 0.1% formic acid. Pumps were operated at a flow rate of 0.4 ml/min for 5 min using gradient elution. Peak area counts of analyte and IS were measured using TSQ Vantage triple-quadrupole mass spectrometric detector, equipped with an electrospray probe set in a positive ionization mode. Selected reaction monitoring was used for the quantitation of DRP-104 by monitoring the transition pair of mass/charge ratio (*m*/*z*) 414.169 to 285.185/130.058, and similarly, losartan was monitored by the transition pair *m*/*z* 422.871 to 207.050/180.026. DON liberated from DRP-104 was determined using our previously reported method (*74*).

MET-ID was performed on a Dionex UPLC system coupled with Q Exactive Focus Orbitrap mass spectrometer (Thermo Fisher Scientific Inc., Waltham, MA). The separation of analytes was achieved using the Agilent Eclipse Plus column (100 mm × 2.1 mm inside diameter; maintained at 35°C) packed with a 1.8-μm C18 stationary phase. The mobile phase consisted of 0.1% formic acid in water and 0.1% formic acid in acetonitrile. Pumps were operated at a flow rate of 0.3 ml/min for 7 min using gradient elution. The mass spectrometer controlled by Xcalibur software 4.0.27.13 (Thermo Fisher Scientific) was operated with a heated electrospray ionization (ESI) ion source in a positive ionization mode. Metabolites were identified in the full-scan mode (from *m*/*z* 50 to 1600) by comparing $t = 0$ samples with $t = 60$ min samples, and structures were proposed on the basis of the accurate mass information.

PK in mice

C57BL/6/$CES1^{-/-}$ mice were obtained as a gift from the United States Army Medical Research Institute of Chemical Defense, Maryland, USA, and breeding was performed in the Johns Hopkins animal facility. PK studies in C57BL/6/$CES1^{-/-}$ mice were conducted according to protocols reviewed and approved by the Johns Hopkins IACUC in compliance with the Association for Assessment and Accreditation of Laboratory Animal Care International (AAALAC) and the Public Health Service Policy on the Humane Care and Use of Laboratory Animals (PHS Policy).

Briefly, naïve male and female C57BL/6/$CES1^{-/-}$ mice (weighing between 25 and 30 g) at 6 to 8 weeks of age were used. The animals were maintained on a 12-hour light/12-hour dark cycle with ad libitum access to food and water. EL4 mouse lymphoma cells were obtained from the American Type Culture Collection, maintained as previously described (*74*), and, upon confluence, were injected subcutaneously (0.3×10^6 cells) in the right flank of the mice, and tumor growth was monitored. Tumor volume was calculated using the formula $V = (L \times W)/2$, where V is the tumor volume, W is the tumor width, and L is the tumor length, and mice with a mean tumor volume around 400 mm^3 were considered for the PK study ($n = 3$ mice per time point). Before dosing, the interscapular region was wiped with alcohol gauze. DRP-104 formulation was prepared freshly on the day of the study in a vehicle containing ethanol:Tween 80:saline (5:10:85, v/v/v) and was administered to mice as a single subcutaneous dose of 2.6 mg/kg (1 mg/kg DON equivalent dose). The mice were euthanized with carbon dioxide at specified time points after drug administration, and blood samples (~0.8 ml) were collected in heparinized microtubes by cardiac puncture. GI tissue and tumors were removed and flash-frozen on dry ice. Blood samples were centrifuged at a temperature of 4°C at 3000*g* for 10 min. Plasma (~300 μl) was collected in heparin-coated polypropylene tubes, and all plasma and tissue samples were stored at −80°C until bioanalysis.

DON bioanalysis was performed as we have previously described (*37*, *74*). Briefly, DON was extracted from samples by protein precipitation using methanol. Standards, quality controls, and samples were mixed in tissue (5 μl/mg) with methanol containing 10 μM glutamate-d_5 (IS) in low-retention microcentrifuge tubes, and tissues were mechanically homogenized. Samples were vortex-mixed and centrifuged at 16,000*g* for 5 min at 4°C. The supernatant (100 μl) was transferred to a new tube and dried under vacuum at 45°C for 45 min. To each tube, 25 μl of 0.2 M sodium bicarbonate buffer (pH 9.0) and 50 μl of 10 mM dabsyl chloride were added. After vortex mixing, samples were incubated at 60°C for 15 min to derivatize,

followed by centrifugation at 16,000*g* for 5 min at 4°C. A 20-μl aliquot of the supernatant was transferred to a 96-well plate and diluted with 80 μl of water. DON was analyzed by injecting 4 μl on a Dionex UPLC system coupled with a Q Exactive Focus Orbitrap mass spectrometer (Thermo Fisher Scientific Inc., Waltham, MA). Separation was achieved at 35°C using an Agilent Eclipse Plus column (100 mm × 2.1 mm inside diameter) packed with a 1.8-μm C18 stationary phase. The mobile phase consisted of 0.1% formic acid in water and 0.1% formic acid in acetonitrile. Pumps were operated at a flow rate of 0.3 ml/min for 3.5 min using gradient elution. The mass spectrometer was operated with a heated ESI ion source in a positive ionization mode. Quantification was performed in a parallel-reaction monitoring mode. Calibration curves were constructed over the range of 0.03 to 100 nmol/ml plasma or nmol/g tissue with naïve sample-matched matrix.

For quantifying DRP-104 levels, plasma samples (25 μl) were extracted using a protein precipitation method by addition of 150 μl of acetonitrile containing IS (losartan, 0.5 μM), followed by vortex mixing for 30 s and then centrifugation at 10,000*g* for 10 min at 4°C. The GI and tumor tissues were diluted 1:2 (w/v) with acetonitrile containing the IS (0.5 μM), homogenized, then vortex-mixed, and centrifuged at 10,000*g* for 10 min at 4°C. A 25-μl aliquot of the supernatant was diluted with 25 μl of water and transferred to 250 μl of polypropylene autosampler vials and analyzed using LC-MS/MS. Calibration curves were prepared with naïve plasma, GI, and tumor tissues ranging from 0.001 to 50 nmol/ml. Linear regression with 1/(nominal concentration) weighting factor was used for fitting the calibration curve. A correlation coefficient of greater than 0.99 was considered acceptable in the analytical runs for all analyses.

Mean plasma and tissue concentrations of DRP-104 and DON were analyzed using noncompartmental analysis method as implemented in the computer software program Phoenix WinNonlin version 8.2 (Certara USA Inc., Princeton, NJ). The maximum plasma and tissue concentration (C_{max}) and time to C_{max} (T_{max}) were the observed values. The area under the plasma and tissue concentration-time curve (AUC) values were calculated to the last quantifiable sample ($AUC_{0\text{-}t}$) using the log-linear trapezoidal rule.

Metabolic stability studies using protease inhibitors

The stability analysis of DRP-104 was performed using EL4 tumor homogenates and mouse intestinal homogenates with or without the presence of protease class inhibitors (Cell Signaling Technology, MA). Briefly, washed tissues were diluted 10-fold in 0.1 M potassium phosphate buffer and homogenized using a probe sonicator. Each of the crude homogenate was then aliquoted to 1 ml and was spiked with specific concentrations of individual protease class inhibitor (1 mM Pefabloc, 1.0 mM PMSF, 0.8 μM aprotinin, 10 μM Bestatin, 10 μM E64, 100 μM leupeptin, 1.0 μM pepstatin A, 1× protease cocktail, and 500 μM dichlorvos) or vehicle (control) followed by an incubation of 15 min in an orbital shaker at 37°C. The incubated homogenate was then spiked with 5 μM of DRP-104 and incubated in an orbital shaker at 37°C for 1 hour (in triplicate). Sample from each incubation at predetermined time points (0 min, 30 min, and 1 hour) was quenched with three volumes of acetonitrile containing IS (0.5 μM). Samples were vortex-mixed for 30 s and centrifuged at 10,000*g* for 10 min at 4°C. Disappearance of DRP-104 was monitored over time using LC-MS/MS as detailed in the "Metabolic stability studies" section. MET-ID was performed on a Dionex UPLC system coupled with Q Exactive Focus Orbitrap mass spectrometer as detailed in the "Metabolic stability studies" section. Metabolites were identified in the full-scan mode (from *m*/*z* 50 to 1600) by comparing $t = 0$ samples with $t = 60$ min samples, and structures were proposed on the basis of the accurate mass information.

Antitumor and tolerability evaluation

C57BL/6/CES1$^{-/-}$ EL4 tumor-bearing mice were used for efficacy studies following either DON (Sigma-Aldrich, St. Louis, MO) or DRP-104 administration by intravenous or subcutaneous route. Briefly, EL4 cells were injected subcutaneously (0.3×10^6) in the right flank, and tumor growth was monitored as described above. For the intravenous cohort, the animals with a mean tumor volume of approximately 400 mm^3 were randomized into three groups—vehicle, DON (1 mg/kg), and DRP-104 (1 mg/kg DON equivalent dose; $n = 8$ per group). The animals were dosed for 5 days per week for 2 weeks with simultaneous recording of the tumor volume using Vernier calipers (VWR, USA), body weight, and mortality. The study was continued until complete regression of the tumor was observed in the DON- and DRP-104–treated groups. At the end of the study, blood samples (for CBC) and GI tissues (for histopathology) were collected for toxicity evaluation. Similarly, for the subcutaneous dosing cohort, DRP-104 was dosed at 0.1, 0.3, and 1 mg/kg (DON equivalent dose) 5 days per week with simultaneous recording of the tumor volume and body weight. Again, GI tissue was collected for histopathology. In all cases, mice were sacrificed when the tumor reached >4000 mm^3, became ulcerated or necrotic, or caused functional deficits.

GI histopathology

GI tissues were isolated from the mice following the completion of the antitumor and tolerability studies and fixed in 10% formalin before being transferred to 70% ethanol. Samples were then shipped to IDEXX Bioanalytics (Columbia, MO) to be embedded in paraffin, sectioned, and stained for hematoxylin and eosin. Blinded histopathological review was performed, both by IDEXX and internally at Johns Hopkins Medical Institute (JHMI), followed by quantification of histological changes using a scoring rubric adapted from Erben *et al.* (*75*) that included metrics of inflammation (0 to 3) and architectural change (0 to 3), as detailed in fig. S10. Final images were acquired on a Zeiss LSM 800 microscope (Zeiss, Germany) using the bright-field settings and a magnification of ×20.

Anti-PD-1 combination studies

MC38 cells were donated by CORVUS Pharmaceuticals (Burlingame, CA). C57BL/6/CES1$^{-/-}$ mice ($n = 4$ male and 3 female mice per group; four groups) were injected subcutaneously on the right flank with 5×10^5 MC38 tumor cells cultured in Dulbecco's Modified Eagle's Medium (DMEM)–based medium. Mice were monitored for approximately 10 days to achieve the desired mean tumor volume (~400 mm^3). Animals were randomized in four groups ($n = 7$ mice per group): (a) vehicle; (b) four doses of 100 μg of anti-PD-1 intraperitoneally on days 10, 12, 14, and 16 after inoculation; (c) DRP-104 at 0.8 mg/kg subcutaneously 5 days a week for 4 weeks; and (d) combination of group b and group c. Tumor volume was calculated as described above. Mice were sacrificed when the tumor reached >4000 mm^3 in any dimension, became ulcerated or necrotic, or caused functional deficits. Unless otherwise specified, average tumor volume is depicted up until the time of the first sacrifice. For tumor rechallenge experiments, CES1 knockout mice [treated with a lower dose of DRP-104 (0.26 and 1 mg/kg)] that had undetectable tumors

for >60 days were reinoculated with MC38 on the opposite flank. Measurements were performed starting on day 6 after reinoculation, and no further treatment was given. For CD8 depletion studies (also performed in CES1 knockout mice), anti-mouse CD8β (clone 53-5.8) and isotype control (rat immunoglobulin G1, clone HRPN) were administered (5 mg/kg) on the day before implantation, the day after implantation, and weekly thereafter. CD8 depletion was confirmed by flow cytometry.

TIL isolation

For TIL isolation experiments, mice were treated with DRP-104 (0.8 mg/kg per day) in 100 μl for days 21 to 24. For antigen-specific T cell evaluation, OVA-expressing MC38 tumors were used in the same manner as described above. Tumors were harvested from sacrificed mice on day 24 after tumor inoculation. Explanted tumors were manually disrupted before incubating in collagenase type I (Gibco) and deoxyribonuclease (DNase) (Roche) in RPMI for 30 min at 37°C. Tumor mixtures, spleens, and nondraining (left inguinal) and draining (right inguinal) lymph nodes were dissociated through a 70-μm filter and washed with phosphate-buffered saline (PBS). Tumor suspensions were pelleted and resuspended in 40% Percoll solution, which was underlaid with 80% Percoll in a 15-ml conical flask. After centrifugation at 2000*g* for 30 min, the middle layer was removed, washed in PBS, and counted.

Flow cytometry and intracellular staining

Antibodies against the following proteins were purchased from BD Biosciences: CD69 (H1.2F3), CD122 (9TM-beta1), BCL-6 (K112-91), and CD127 (M1/69). Antibodies against the following proteins were purchased from eBioscience: CD44 (IM7), EOMES (Dan11mag), Ki-67 (SolA15), KLRG1 (2F1), and T-bet (eBio4B10). Antibodies against the following proteins were purchased from BioLegend: CD4 (RM4-5), CD27 (LG7F9), CD45 (30-F11), CD62L (MEL-14), PD-1 (29F.1A12), and Bcl2 (BCL/10C4). Phycoerythrin (PE)–labeled tetramer (MBL) staining for OVA-specific T cells was performed at a dilution of 1:50 before surface staining. Normal anti–TCF1/7 was purchased from Cell Signaling Technology. Fc Block (2.4G2) was purchased from BioXCell. Fixable viability dye eFluor780 was purchased from eBioscience; near-infrared fixable viability dye was purchased from Invitrogen. Flow cytometry experiments were performed on FACSCelesta (BD Biosciences) and analyzed using FlowJo software (v.10.3, Tree Star Inc.). Intracellular staining was performed with eBioscience Foxp3/Transcription Factor Staining Buffer Set (Invitrogen).

Global metabolomic and $^{13}C_5$-glutamine flux analysis

Metabolomic analysis was conducted on a satellite group of C57BL/6/CES1$^{-/-}$ mice (n = 5 per group) bearing EL4 tumors treated with DRP-104 subcutaneously (0.3 mg/kg DON equivalent/day for 5 days). Tumors were harvested and flash-frozen in liquid nitrogen. Global metabolite profiling on tumors was performed by Metabolon Inc. (Durham, NC) using UPLC-MS/MS. Individual tumors were subjected to methanol extraction and then split into aliquots for analysis. The global biochemical profiling method is composed of four arms consisting of reversed-phase chromatography positive ionization methods optimized for hydrophilic compounds (LC-MS Pos Polar) and hydrophobic compounds (LC-MS Pos Lipid), reversed-phase chromatography with negative ionization conditions (LC-MS Neg), as well as a HILIC remove chromatography method coupled to negative ionization (LC-MS Polar) (*76*). All of the methods alternated between full-scan MS and data-dependent MSn scans. The scan range generally covered 70 to 1000 m/z. Metabolites were identified by automated comparison of the ion features in the experimental samples to a reference library of chemical standard entries (*77*). LC-MS data on polar compounds were analyzed at Johns Hopkins using Metaboanalyst 4.0 (*78*). Features with >51% missing data were removed, and other missing variables were replaced by a small value. Peak intensities were normalized to tissue mass-extracted, log-transformed, and mean-centered before statistical analysis.

To assess the effect of DRP-104 on influx of glutamine-derived metabolites to the TCA cycle, we performed in vivo $^{13}C_5$-glutamine (Sigma-Aldrich, St. Louis, MO) flux analysis on mice bearing EL4 tumors treated with vehicle or DRP-104. Briefly, CES1$^{-/-}$ mice with established EL4 tumors were treated with vehicle or DRP-104 (0.3 mg/kg DON equivalent, subcutaneously) for 3 days. On day 4, mice received treatment DRP-104 treatment or vehicle followed by two tail vein injections of $^{13}C_5$-glutamine (200 mM dissolved in PBS buffer) at 30 and 45 min after dose. Mice were euthanized 15 min after the second dose (1 hour following DRP-104 treatment), and tumors were harvested and flash-frozen. For analyses, metabolites were extracted from tissues (50 to 100 mg) in methanol:water (80:20, v/v) after homogenization. Samples were vortex-mixed and stored at −80°C for at least 2 hours to allow protein precipitation. Samples were thawed and centrifuged (15,000*g* for 10 min), and supernatant was isolated and dried under nitrogen gas, followed by resuspension in 50% acetonitrile solution. LC-MS–based metabolomics profiling was performed on an Agilent LC-MS system. Chromatographic separations were performed using an Agilent 1290 UPLC system with a well-plate autosampler (Agilent, Santa Clara, CA, USA). An ion-pairing method was used using a C18 column (Agilent Zorbax Extend C18, 2.1 mm × 150 mm, 1.8 μm) with tributylamine as an ion-pairing agent. The LC parameters were as follows: autosampler temperature, 4°C; injection volume, 2 μl; column temperature, 40°C; and flow rate, 0.25 ml/min. The solvents consisted of solvent A, 97% water/3% methanol containing 5 mM tetrabutyl ammonium hydroxide (TBA) and 5 mM acetic acid, and solvent B, methanol containing 5 mM TBA and 5 mM acetic acid. Analytes were separated using a nonlinear gradient from 0% B to 99% B in 22 min with 5 min of postrun time. Samples were detected on a 6520 accurate-mass quadrupole time-of-flight LC-MS system (Agilent) equipped with a dual ESI ion source, operated in a negative-ion mode for metabolic profiling. Data were acquired with MassHunter Acquisition software. A metabolite database with retention times based on the ion-pairing method was developed using Agilent MassHunter PCDL manager software. The isotopologue peak extractions, isotope incorporation analysis, and natural abundance correction were achieved by Agilent MassHunter Profinder software.

Statistical analysis

Animals were randomly assigned to treatment groups, and all experimental data were acquired under blinded conditions. Survival was analyzed by Kaplan-Meier curves and log-rank test, followed by the Gehan-Breslow-Wilcoxon test for multiple comparisons. Comparisons between two treatment groups were conducted using an unpaired Student's t test. Data are expressed as means ± SEM or SD. Probability values (P) less than 0.05 were considered to be significant in all experiments. All data were analyzed with GraphPad Prism 8.1.1.

SUPPLEMENTARY MATERIALS

Supplementary material for this article is available at https://science.org/doi/10.1126/sciadv.abq5925

REFERENCES AND NOTES

1. D. Hanahan, R. A. Weinberg, Hallmarks of cancer: The next generation. *Cell* **144**, 646–674 (2011).
2. K. M. Lemberg, S. S. Gori, T. Tsukamoto, R. Rais, B. S. Slusher, Clinical development of metabolic inhibitors for oncology. *J. Clin. Invest.* **132**, e148550 (2022).
3. C. Hirayama, K. Suyama, Y. Horie, K. Tanimoto, S. Kato, Plasma amino acid patterns in hepatocellular carcinoma. *Biochem. Med. Metab. Biol.* **38**, 127–133 (1987).
4. R. J. DeBerardinis, A. Mancuso, E. Daikhin, I. Nissim, M. Yudkoff, S. Wehrli, C. B. Thompson, Beyond aerobic glycolysis: Transformed cells can engage in glutamine metabolism that exceeds the requirement for protein and nucleotide synthesis. *Proc. Natl. Acad. Sci. U.S.A.* **104**, 19345–19350 (2007).
5. J. S. Flier, M. M. Mueckler, P. Usher, H. F. Lodish, Elevated levels of glucose transport and transporter messenger RNA are induced by *ras* or *src* oncogenes. *Science* **235**, 1492–1495 (1987).
6. H. Ying, A. C. Kimmelman, C. A. Lyssiotis, S. Hua, G. C. Chu, E. Fletcher-Sananikone, J. W. Locasale, J. Son, H. Zhang, J. L. Coloff, H. Yan, W. Wang, S. Chen, A. Viale, H. Zheng, J. H. Paik, C. Lim, A. R. Guimaraes, E. S. Martin, J. Chang, A. F. Hezel, S. R. Perry, J. Hu, B. Gan, Y. Xiao, J. M. Asara, R. Weissleder, Y. A. Wang, L. Chin, L. C. Cantley, R. A. DePinho, Oncogenic Kras maintains pancreatic tumors through regulation of anabolic glucose metabolism. *Cell* **149**, 656–670 (2012).
7. D. Meynial-Denis, *Glutamine: Biochemistry, Physiology, and Clinical Applications* (CRC Press, 2017).
8. Y.-K. Choi, K.-G. Park, Targeting glutamine metabolism for cancer treatment. *Biomol. Ther.* **26**, 19–28 (2018).
9. D. R. Wise, C. B. Thompson, Glutamine addiction: A new therapeutic target in cancer. *Trends Biochem. Sci.* **35**, 427–433 (2010).
10. K. Thangavelu, C. Q. Pan, T. Karlberg, G. Balaji, M. Uttamchandani, V. Suresh, H. Schuler, B. C. Low, J. Sivaraman, Structural basis for the allosteric inhibitory mechanism of human kidney-type glutaminase (KGA) and its regulation by Raf-Mek-Erk signaling in cancer cell metabolism. *Proc. Natl. Acad. Sci. U.S.A.* **109**, 7705–7710 (2012).
11. R. J. Rosenbluth, D. A. Cooney, H. N. Jayaram, H. A. Milman, E. R. Homan, DON, CONV and DONV-II. Inhibition of L-asparagine synthetase in vivo. *Biochem. Pharmacol.* **25**, 1851–1858 (1976).
12. R. K. Barclay, M. A. Phillipps, Effects of 6-diazo-5-oxo-L-norleucine and other tumor inhibitors on the biosynthesis of nicotinamide adenine dinucleotide in mice. *Cancer Res.* **26**, 282–286 (1966).
13. G. S. Ahluwalia, J. L. Grem, Z. Hao, D. A. Cooney, Metabolism and action of amino acid analog anti-cancer agents. *Pharmacol. Ther.* **46**, 243–271 (1990).
14. B. Levenberg, I. Melnick, J. M. Buchanan, Biosynthesis of the purines. XV. The effect of aza-L-serine and 6-diazo-5-oxo-L-norleucine on inosinic acid biosynthesis de novo. *J. Biol. Chem.* **225**, 163–176 (1957).
15. M. L. Eidinoff, J. E. Knoll, B. Marano, L. Cheong, Pyrimidine studies: I. Effect of DON (6-diazo-5-oxo-L-norleucine) on incorporation of precursors into nucleic acid pyrimidines. *Cancer Res.* **18**, 105–109 (1958).
16. L. M. Pinkus, [45] Glutamine binding sites, in *Methods in Enzymology* (Elsevier, 1977), vol. 46, pp. 414–427.
17. H. W. Dion, S. A. Fusari, Z. L. Jakubowski, J. G. Zora, Q. R. Bartz, 6-Diazo-5-oxo-L-norleucine, a new tumor-inhibitory substance. II. Isolation and characterization. *J. Am. Chem. Soc.* **78**, 3075–3077 (1956).
18. R. D. Leone, L. Zhao, J. M. Englert, I. M. Sun, M. H. Oh, I. H. Sun, M. L. Arwood, I. A. Bettencourt, C. H. Patel, J. Wen, A. Tam, R. L. Blosser, E. Prchalova, J. Alt, R. Rais, B. S. Slusher, J. D. Powell, Glutamine blockade induces divergent metabolic programs to overcome tumor immune evasion. *Science* **366**, 1013–1021 (2019).
19. G. B. Magill, W. P. Myers, H. C. Reilly, R. C. Putnam, J. W. Magill, M. P. Sykes, G. C. Escher, D. A. Karnofsky, J. H. Burchenal, Pharmacological and initial therapeutic observations on 6-diazo-5-oxo-L-norleucine (DON) in human neoplastic disease. *Cancer* **10**, 1138–1150 (1957).
20. M. P. Sullivan, J. A. Nelson, S. Feldman, B. Van Nguyen, Pharmacokinetic and phase I study of intravenous DON (6-diazo-5-oxo-L-norleucine) in children. *Cancer Chemother. Pharmacol.* **21**, 78–84 (1988).
21. R. H. Earhart, D. J. Amato, A. Y. Chang, E. C. Borden, M. Shiraki, M. E. Dowd, R. L. Comis, T. E. Davis, T. J. Smith, Phase II trial of 6-diazo-5-oxo-L-norleucine versus aclacinomycin-A in advanced sarcomas and mesotheliomas. *Invest. New Drugs* **8**, 113–119 (1990).
22. A. Rahman, F. P. Smith, P. T. Luc, P. V. Woolley, Phase I study and clinical pharmacology of 6-diazo-5-oxo-L-norleucine (DON). *Invest. New Drugs* **3**, 369–374 (1985).
23. R. T. Eagan, S. Frytak, W. C. Nichols, E. T. Creagan, J. N. Ingle, Phase II study on DON in patients with previously treated advanced lung cancer. *Cancer Treat. Rep.* **66**, 1665–1666 (1982).
24. R. H. Earhart, J. M. Koeller, H. L. Davis, Phase I trial of 6-diazo-5-oxo-L-norleucine (DON) administered by 5-day courses. *Cancer Treat. Rep.* **66**, 1215–1217 (1982).
25. J. S. Kovach, R. T. Eagan, G. Powis, J. Rubin, E. T. Creagan, C. G. Moertel, Phase I and pharmacokinetic studies of DON. *Cancer Treat. Rep.* **65**, 1031–1036 (1981).
26. G. Lynch, N. Kemeny, E. Casper, Phase II evaluation of DON (6-diazo-5-oxo-L-norleucine) in patients with advanced colorectal carcinoma. *Am. J. Clin. Oncol.* **5**, 541–543 (1982).
27. A. A. Ovejera, D. P. Houchens, R. Catane, M. A. Sheridan, F. M. Muggia, Efficacy of 6-diazo-5-oxo-L-norleucine and *N*-[*N*-γ-glutamyl-6-diazo-5-oxo-norleucinyl]-6-diazo-5-oxo-norleucine against experimental tumors in conventional and nude mice. *Cancer Res.* **39**, 3220–3224 (1979).
28. J. Rubin, S. Sorensen, A. J. Schutt, G. A. van Hazel, M. J. O'Connell, C. G. Moertel, A phase II study of 6-diazo-5-oxo-L-norleucine (DON, NSC-7365) in advanced large bowel carcinoma. *Am. J. Clin. Oncol.* **6**, 325–326 (1983).
29. L. M. Shelton, L. C. Huysentruyt, T. N. Seyfried, Glutamine targeting inhibits systemic metastasis in the VM-M3 murine tumor model. *Int. J. Cancer* **127**, 2478–2485 (2010).
30. G. S. Tarnowski, C. C. Stock, Effects of combinations of azaserine and of 6-diazo-5-oxo-L-norleucine with purine analogs and other antimetabolites on the growth of two mouse mammary carcinomas. *Cancer Res.* **17**, 1033–1039 (1957).
31. R. Catane, D. D. Von Hoff, D. L. Glaubiger, F. M. Muggia, Azaserine, DON, and azotomycin: Three diazo analogs of L-glutamine with clinical antitumor activity. *Cancer Treat. Rep.* **63**, 1033–1038 (1979).
32. M. Sullivan, E. Beatty Jr., C. Hyman, M. Murphy, M. Pierce, N. Severo, A comparison of the effectiveness of standard dose 6-mercaptopurine, combination 6-mercaptopurine and DON, and high-loading 6-mercaptopurine therapies in treatment of the acute leukemias of childhood: Results of a coperative study. *Cancer Chemother. Rep.* **18**, 83–95 (1962).
33. C. T. Hensley, A. T. Wasti, R. J. DeBerardinis, Glutamine and cancer: Cell biology, physiology, and clinical opportunities. *J. Clin. Invest.* **123**, 3678–3684 (2013).
34. Calithera, Calithera Biosciences announces decision to discontinue KEAPSAKE clinical trial (2021).
35. C. Wyatt, J. M. Baeten, Tenofovir alafenamide for HIV infection: Is less more? *Lancet* **385**, 2559–2560 (2015).
36. M. T. Nedelcovych, L. Tenora, B.-H. Kim, J. Kelschenbach, W. Chao, E. Hadas, A. Jancarik, E. Prchalova, S. C. Zimmermann, R. P. Dash, A. J. Gadiano, C. Garrett, G. Furtmuller, B. Oh, G. Brandacher, J. Alt, P. Majer, D. J. Volsky, R. Rais, B. S. Slusher, *N*-(Pivaloyloxy) alkoxy-carbonyl prodrugs of the glutamine antagonist 6-diazo-5-oxo-L-norleucine (DON) as a potential treatment for HIV associated nseurocognitive disorders. *J. Med. Chem.* **60**, 7186–7198 (2017).
37. R. Rais, A. Jančařík, L. Tenora, M. Nedelcovych, J. Alt, J. Englert, C. Rojas, A. Le, A. Elgogary, J. Tan, L. Monincová, K. Pate, R. Adams, D. Ferraris, J. Powell, P. Majer, B. S. Slusher, Discovery of 6-diazo-5-oxo-L-norleucine (DON) prodrugs with enhanced CSF delivery in monkeys: A potential treatment for glioblastoma. *J. Med. Chem.* **59**, 8621–8633 (2016).
38. K. Y. Choi, M. Swierczewska, S. Lee, X. Chen, Protease-activated drug development. *Theranostics* **2**, 156–178 (2012).
39. N. Ueki, S. Lee, N. S. Sampson, M. J. Hayman, Selective cancer targeting with prodrugs activated by histone deacetylases and a tumour-associated protease. *Nat. Commun.* **4**, 2735 (2013).
40. P. L. Carl, P. K. Chakravarty, J. A. Katzenellenbogen, M. J. Weber, Protease-activated "prodrugs" for cancer chemotherapy. *Proc. Natl. Acad. Sci. U.S.A.* **77**, 2224–2228 (1980).
41. A. G. Thomas, C. Rojas, C. Tanega, M. Shen, A. Simeonov, M. B. Boxer, D. S. Auld, D. V. Ferraris, T. Tsukamoto, B. S. Slusher, Kinetic characterization of ebselen, chelerythrine and apomorphine as glutaminase inhibitors. *Biochem. Biophys. Res. Commun.* **438**, 243–248 (2013).
42. B. Li, M. Sedlacek, I. Manoharan, R. Boopathy, E. G. Duysen, P. Masson, O. Lockridge, Butyrylcholinesterase, paraoxonase, and albumin esterase, but not carboxylesterase, are present in human plasma. *Biochem. Pharmacol.* **70**, 1673–1684 (2005).
43. E. G. Duysen, F. Koentgen, G. R. Williams, C. M. Timperley, L. M. Schopfer, D. M. Cerasoli, O. Lockridge, Production of ES1 plasma carboxylesterase knockout mice for toxicity studies. *Chem. Res. Toxicol.* **24**, 1891–1898 (2011).
44. K. M. Lemberg, L. Zhao, Y. Wu, V. Veeravalli, J. Alt, J. M. H. Aguilar, R. P. Dash, J. Lam, L. Tenora, C. Rodriguez, M. T. Nedelcovych, C. Brayton, P. Majer, J. O. Blakeley, R. Rais, B. S. Slusher, The novel glutamine antagonist prodrug JHU395 has antitumor activity in malignant peripheral nerve sheath tumor. *Mol. Cancer Ther.* **19**, 397–408 (2020).
45. J. Alt, S. S. Gori, K. M. Lemberg, A. Pal, V. Veeravalli, Y. Wu, J. M. H. Aguilar, R. P. Dash, L. Tenora, P. Majer, Q. Sun, B. S. Slusher, R. Rais, Glutamine antagonist GA-607 causes a dramatic accumulation of FGAR which can be used to monitor target engagement. *Curr. Drug Metab.* **22**, 735–745 (2021).
46. A. Le, A. N. Lane, M. Hamaker, S. Bose, A. Gouw, J. Barbi, T. Tsukamoto, C. J. Rojas, B. S. Slusher, H. Zhang, L. J. Zimmerman, D. C. Liebler, R. J. Slebos, P. K. Lorkiewicz, R. M. Higashi, T. W. Fan, C. V. Dang, Glucose-independent glutamine metabolism via TCA cycling for proliferation and survival in B cells. *Cell Metab.* **15**, 110–121 (2012).

47. R. J. DeBerardinis, T. Cheng, Q's next: The diverse functions of glutamine in metabolism, cell biology and cancer. *Oncogene* **29**, 313–324 (2010).
48. D. A. Tennant, R. V. Durán, E. Gottlieb, Targeting metabolic transformation for cancer therapy. *Nat. Rev. Cancer* **10**, 267–277 (2010).
49. K. M. Lemberg, J. J. Vornov, R. Rais, B. S. Slusher, We're not "DON" yet: Optimal dosing and prodrug delivery of 6-diazo-5-oxo-L-norleucine. *Mol. Cancer Ther.* **17**, 1824–1832 (2018).
50. F. Kratz, K. Abu Ajaj, A. Warnecke, Anticancer carrier-linked prodrugs in clinical trials. *Expert Opin. Investig. Drugs* **16**, 1037–1058 (2007).
51. C. Souza, D. S. Pellosi, A. C. Tedesco, Prodrugs for targeted cancer therapy. *Expert Rev. Anticancer Ther.* **19**, 483–502 (2019).
52. R. Mahato, W. Tai, K. Cheng, Prodrugs for improving tumor targetability and efficiency. *Adv. Drug Deliv. Rev.* **63**, 659–670 (2011).
53. H. He, L. Sun, J. Ye, E. Liu, S. Chen, Q. Liang, M. C. Shin, V. C. Yang, Enzyme-triggered, cell penetrating peptide-mediated delivery of anti-tumor agents. *J. Control. Release* **240**, 67–76 (2016).
54. Y. J. Zhong, L. H. Shao, Y. Li, Cathepsin B-cleavable doxorubicin prodrugs for targeted cancer therapy (Review). *Int. J. Oncol.* **42**, 373–383 (2013).
55. L.-H. Shao, S.-P. Liu, J.-X. Hou, Y.-H. Zhang, C.-W. Peng, Y.-J. Zhong, X. Liu, X.-L. Liu, Y.-P. Hong, R. A. Firestone, Y. Li, Cathepsin B cleavable novel prodrug Ac-Phe-Lys-PABC-ADM enhances efficacy at reduced toxicity in treating gastric cancer peritoneal carcinomatosis: An experimental study. *Cancer* **118**, 2986–2996 (2012).
56. J. Rautio, N. A. Meanwell, L. Di, M. J. Hageman, The expanding role of prodrugs in contemporary drug design and development. *Nat. Rev. Drug Discov.* **17**, 559–587 (2018).
57. A. Najjar, A. Najjar, R. Karaman, Newly developed prodrugs and prodrugs in development; an insight of the recent years. *Molecules* **25**, 884 (2020).
58. M. D. Kramer, P. Robinson, I. Vlodavsky, D. Barz, P. Friberger, Z. Fuks, V. Schirrmacher, Characterization of an extracellular matrix-degrading protease derived from a highly metastatic tumor cell line. *Eur. J. Cancer Clin. Oncol.* **21**, 307–316 (1985).
59. J. F. DiStefano, G. Beck, B. Lane, S. Zucker, Role of tumor cell membrane-bound serine proteases in tumor-induced target cytolysis. *Cancer Res.* **42**, 207–218 (1982).
60. J. A. Joyce, D. Hanahan, Multiple roles for cysteine cathepsins in cancer. *Cell Cycle* **3**, 1516–1519 (2004).
61. S. P. Sanghani, S. K. Quinney, T. B. Fredenburg, Z. J. Sun, W. I. Davis, D. J. Murry, O. W. Cummings, D. E. Seitz, W. F. Bosron, Carboxylesterases expressed in human colon tumor tissue and their role in CPT-11 hydrolysis. *Clin. Cancer Res.* **9**, 4983–4991 (2003).
62. P. D. Senter, K. S. Beam, B. Mixan, A. F. Wahl, Identification and activities of human carboxylesterases for the activation of CPT-11, a clinically approved anticancer drug. *Bioconjug. Chem.* **12**, 1074–1080 (2001).
63. B. Reigner, K. Blesch, E. Weidekamm, Clinical pharmacokinetics of capecitabine. *Clin. Pharmacokinet.* **40**, 85–104 (2001).
64. M. C. Bissery, P. Vrignaud, F. Lavelle, G. G. Chabot, Experimental antitumor activity and pharmacokinetics of the camptothecin analog irinotecan (CPT-11) in mice. *Anticancer Drugs* **7**, 437–460 (1996).
65. I. G. Kirwan, P. M. Loadman, D. J. Swaine, D. A. Anthoney, G. R. Pettit, J. W. Lippert 3rd, S. D. Shnyder, P. A. Cooper, M. C. Bibby, Comparative preclinical pharmacokinetic and metabolic studies of the combretastatin prodrugs combretastatin A4 phosphate and A1 phosphate. *Clin. Cancer Res.* **10**, 1446–1453 (2004).
66. L. Shan, X. Zhuo, F. Zhang, Y. Dai, G. Zhu, B. C. Yung, W. Fan, K. Zhai, O. Jacobson, D. O. Kiesewetter, Y. Ma, G. Gao, X. Chen, A paclitaxel prodrug with bifunctional folate and albumin binding moieties for both passive and active targeted cancer therapy. *Theranostics* **8**, 2018–2030 (2018).
67. A. G. Thomas, C. M. O'Driscoll, J. Bressler, W. Kaufmann, C. J. Rojas, B. S. Slusher, Small molecule glutaminase inhibitors block glutamate release from stimulated microglia. *Biochem. Biophys. Res. Commun.* **443**, 32–36 (2014).
68. B. M. Liederer, R. T. Borchardt, Enzymes involved in the bioconversion of ester-based prodrugs. *J. Pharm. Sci.* **95**, 1177–1195 (2006).
69. K. M. Huttunen, H. Raunio, J. Rautio, Prodrugs—From serendipity to rational design. *Pharmacol. Rev.* **63**, 750–771 (2011).
70. R. H. Mathijssen, R. J. van Alphen, J. Verweij, W. J. Loos, K. Nooter, G. Stoter, A. Sparreboom, Clinical pharmacokinetics and metabolism of irinotecan (CPT-11). *Clin. Cancer Res.* **7**, 2182–2194 (2001).
71. M.-H. Oh, I.-H. Sun, L. Zhao, R. D. Leone, I.-M. Sun, W. Xu, S. L. Collins, A. J. Tam, R. L. Blosser, C. H. Patel, J. M. Englert, M. L. Arwood, J. Wen, Y. Chan-Li, L. Tenora, P. Majer, R. Rais, B. S. Slusher, M. R. Horton, J. D. Powell, Targeting glutamine metabolism enhances tumor-specific immunity by modulating suppressive myeloid cells. *J. Clin. Invest.* **130**, 3865–3884 (2020).
72. N. S. Sharma, V. K. Gupta, V. T. Garrido, R. Hadad, B. C. Durden, K. Kesh, B. Giri, A. Ferrantella, V. Dudeja, A. Saluja, S. Banerjee, Targeting tumor-intrinsic hexosamine biosynthesis sensitizes pancreatic cancer to anti-PD1 therapy. *J. Clin. Invest.* **130**, 451–465 (2020).
73. S. C. Zimmermann, T. Tichý, J. Vávra, R. P. Dash, C. E. Slusher, A. J. Gadiano, Y. Wu, A. Jančařík, L. Tenora, L. Monincová, E. Prchalová, G. J. Riggins, P. Majer, B. S. Slusher, R. Rais, N-substituted prodrugs of mebendazole provide improved aqueous solubility and oral bioavailability in mice and dogs. *J. Med. Chem.* **61**, 3918–3929 (2018).
74. L. Tenora, J. Alt, R. P. Dash, A. J. Gadiano, K. Novotna, V. Veeravalli, J. Lam, Q. R. Kirkpatrick, K. M. Lemberg, P. Majer, R. Rais, B. S. Slusher, Tumor-targeted delivery of 6-diazo-5-oxo-L-norleucine (DON) using substituted acetylated lysine prodrugs. *J. Med. Chem.* **62**, 3524–3538 (2019).
75. U. Erben, C. Loddenkemper, K. Doerfel, S. Spieckermann, D. Haller, M. M. Heimesaat, M. Zeitz, B. Siegmund, A. A. Kühl, A guide to histomorphological evaluation of intestinal inflammation in mouse models. *Int. J. Clin. Exp. Pathol.* **7**, 4557–4576 (2014).
76. A. M. Evans, B. Br, Q. Liu, M. W. Mitchell, R. Rj, H. Dai, S. Sj, C. D. DeHaven, M. Lad, High resolution mass spectrometry improves data quantity and quality as compared to unit mass resolution mass spectrometry in high-throughput profiling metabolomics. *Metabolomics* **4**, 1–3 (2014).
77. C. D. Dehaven, A. M. Evans, H. Dai, K. A. Lawton, Organization of GC/MS and LC/MS metabolomics data into chemical libraries. *J. Cheminform.* **2**, 9 (2010).
78. J. Xia, D. S. Wishart, Using metaboanalyst 3.0 for comprehensive metabolomics data analysis. *Curr. Protoc. Bioinformatics* **55**, 14.10.11–14.10.91 (2016).
79. K. R. Hollinger, X. Zhu, E. S. Khoury, A. G. Thomas, K. Liaw, C. Tallon, Y. Wu, E. Prchalova, A. Kamiya, C. Rojas, S. Kannan, B. S. Slusher, Glutamine antagonist JHU-083 normalizes aberrant hippocampal glutaminase activity and improves cognition in APOE4 mice. *J. Alzheimers Dis.* **77**, 437–447 (2020).

Acknowledgments

Funding: B.S.S., R.R., R.D.L., and J.D.P. were supported by R01CA193895, R01CA229451, and R01NS103927 and the Bloomberg Kimmel Institute for Cancer Immunotherapy. K.M.L. was supported by a CureSearch for Children's Cancer Young Investigator Award. B.S.S. and R.R. were also supported by R01 CA226765. This work was also funded by an institutional support from the Czech of Sciences (RVO 61388963) and by grant LTAUSA18166 by the Ministry of Education, Youth, and Sports of the Czech Republic (program INTER-EXCELLENCE).

Author contributions: R.R., B.S.S., R.D.L., T.S., and J.D.P. conceived and designed the experiments. R.R., B.S.S., R.D.L., K.M.L., and P.M. wrote the manuscript. L.T. synthesized the chemical compounds. A.P., J.L., R.P.D., J.A., K.M.L., J.M.H.A., R.P., Y.W., A.G.T., and M.L.A. conducted the experiments. R.R., L.Z., J.L., K.M.L., C.T., R.P.D., A.P., J.A., Y.W., A.G.T., and M.L.A. analyzed the data. All authors reviewed and approved the manuscript. **Competing interests:** R.R., L.T., P.M., J.D.P., J.A., and B.S.S. are inventors on multiple Johns Hopkins University (JHU) patents covering novel glutamine antagonist prodrugs and their utility. R.R., L.T., P.M., J.A., and B.S.S. are inventors on patent applications related to the DRP-104 composition in the United States (16/754,053), China (201880079030.2), Europe (18864999.0), and Japan (2020-519241) claiming priority to PCT application. PCT/US2018/054581 filed on 5 October 2018 and published as WO 2019/071110. These patents have been licensed to Dracen Pharmaceuticals Inc. R.R., P.M., J.D.P., and B.S.S. are founders of and hold equity in Dracen Pharmaceuticals Inc. B.S.S., J.D.P., and R.R. also serve/d as scientific consultants to Dracen. This arrangement has been reviewed and approved by the JHU in accordance with its conflict-of-interest policies. The authors declare no other competing interests. **Data and materials availability:** All data needed to evaluate the conclusions in the paper are present in the paper and/or the Supplementary Materials. DRP-104 is available through Dracen Pharmaceuticals (https://dracenpharma.com/) pending scientific review and a completed material transfer agreement. Requests for DRP-104 should be submitted to Dracen Pharmaceuticals.

Submitted 18 April 2022
Accepted 27 September 2022
Published 16 November 2022
10.1126/sciadv.abq5925